Heikki Kangas, Heikki Onninen and Seppo Saarelainen

Testing a pavement on thawing, frost-susceptible subgrade with the heavy vehicle simulator

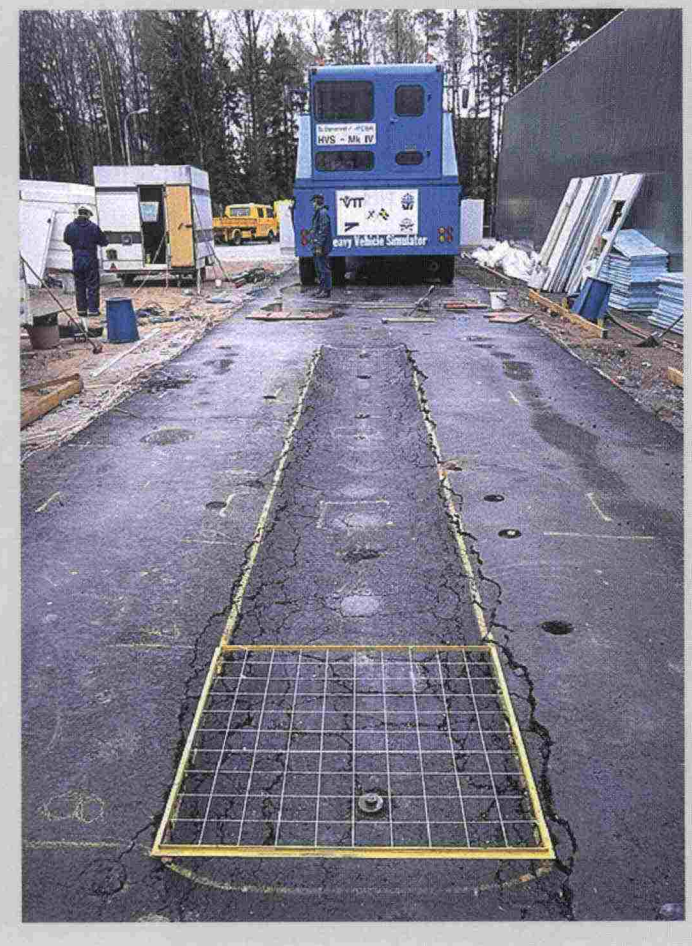

Tielaitos

Finnra Reports
31/2000

Helsinki 2000

Finnish National
Road Administration

VTT

HVS-NORDIC

Finnra Reports
31/2000

Heikki Kangas, Heikki Onninen and Seppo Saarelainen

Testing a pavement on thawing, frost-susceptible subgrade with the heavy vehicle simulator

Finnish National Road Administration
Helsinki 2000

SSN 0788-3722
ISBN 951-726-661-8
TIEL 3200619E

Edita Oy
Helsinki 2000

This publication is available from:
The Finnish National Road Administration, library
Telefax int +358 204 44 2652
http://www.tieh.fi/libr.htm

Finnish National
Road Administration
Opastinsilta 12 A
P.O. Box 33
FIN-00521 HELSINKI, Finland

KANGAS Heikki, ONNINEN Heikki, SAARELAINEN Seppo: Testing a pavement on thawing, frost-susceptible subgrade with the Heavy Vehicle Simulator, Finnish National Road Administration, Finnra reports 31/2000. 69 p. ISBN 951-726-661-8, ISSN 0788-3722, TIEL 3200619E.

Keywords: pavement, subgrade, frost, thaw weakening baring capacity

ABSTRACT

Frost action has very significant effects on pavement properties in cold regions. Within the zones of seasonal frost, the thawing of frost-susceptible subgrade decreases the surface modulus of the overall pavement. This reduces its capability to resist both elastic and permanent deformations under traffic loads, which can cause serious structural damage.

This report presents full-scale accelerated testing of a pavement on thawing, frost-susceptible subgrade. The pavements were tested using the Heavy Vehicle Simulator (HVS-NORDIC) on a test site at Otaniemi in the spring of 1998.

The construction of test pavements, instrumentation, measurements during winter and spring, and the full-scale accelerated testing with the HVS are reported, as well as the main test results and conclusions.

The effects of heavy wheel loads on deformations in frost-susceptible test sections are summarized. The results were based on extensive measurements. The test parameters and loading were also analyzed using numeric and finite element method computer programs, and the results were compared to the measurements.

PREFACE

In Finland, the pavement design is based on thaw, which is the weakest period of the year. Documented data on the behaviour of thawing subgrade under traffic loading has been, so far, scarcely available. Within the Finnish pavement research program (TPPT), it was decided to carry out HVS testing on a pavement on frost-susceptible, thawing subgrade. The aim was to monitor the freezing, frost heaving and thawing of the test pavement and subgrade, and to study the mechanical behaviour of the pavement and subgrade under full-scale wheel loading, in order to evaluate and possibly further develop the mechanistic design approach of pavements in thaw conditions.

This report, "Testing a pavement on thawing, frost-susceptible subgrade with the heavy vehicle simulator", presents the results from the construction, pre-freezing and testing. The investigation was started in 1997, and testing was carried out in the spring of 1998. The report has been written by Mr. Heikki Kangas (M.Sc), Mr. Heikki Onninen (M.Sc) and Mr. Seppo Saarelainen (D.Sc).

The Finnish pavement research program, TPPT, is sponsored by the Finnish National Road Administration (FINNRA). The HVS-NORDIC research is being conducted in co-operation with the Swedish National Road and Transport Research Institute (VTI), and the Swedish National Road Administration (SNRA).

The preliminary planning and design of this test was carried out at VTT Communities and Infrastructure. The test pavement with subgrade was constructed by E.M. Pekkinen Oy and paved by Lemminkäinen Oy. The artificial cooling device was supplied and installed by Huurre-Morus Ltd. The material testing, monitoring and interpreting was performed by VTT staff. The authors express sincere thanks to all the participating bodies and persons.

Espoo 31.12.1999 Seppo Saarelainen

TABLE OF CONTENTS

LIST OF ABBREVIATION AND SYMBOLS

APT	Accelerated Pavement Testing
FINNRA	Finnish National Road Administration
HVS	Heavy Vehicle Simulator
SNRA	Swedish National Road Administration
TPPT	Finnish National Road Structures Research Programme
VTI	Swedish Road and Transport Research Institute
VTT	Technical Research Centre of Finland
AC	asphalt concrete
E	modulus of elasticity, MN/m^2
ESWL	equivalent single-wheel load
F	freezing index, Kh
FEM	finite element method
FWD	falling weight deflectometer
G	modulus of shear, MN/m^2
Hu	humus content, %
I_p	plasticity index ($=w_p-w_l$)
K	bulk modulus, MN/m^2
MLT	multi-layered elastic theory
N	number of load repetitions, allowable number of load repetitions
PSI	present serviceability index
r	radius of circle or plate, m
SP	frost heave coefficient (segregation potential), mm^2/Kh
S_r	degree of saturation
T	temperature, K, °C
c	cohesion, kN/m^2
e	void ratio
h	thickness, m, mm
s_k	shear strength, kN/m^2
t	time, s, min, h, d
u	rut depth, mm
w	water content, %
w_l	liquid limit, %
w_p	plastic limit, %
z	depth, m, mm
Δ_{tot}	deflection of pavement surface due to wheel load, mm
Δ_p	permanent deformation of overall pavement due to wheel load, increase of rut depth, mm/overpass
Δ_{sub}	deflection of subgrade surface due to wheel load, mm
ε	elastic (compressive) strain
ε_p	permanent, irreversible strain
ε_{sub}	vertical compressive strain on the surface of subgrade

ϕ	angle of internal friction, ^{o}
γ	shear strain
γ_{sub}	shear strain on the surface of subgrade
γ	unit weight of material, kN/m^3
γ_d	dry unit weight of material, kN/m^3
ν	Poisson ratio
σ'	effective stress, kN/m^2
σ_d	deviator stress, kN/m^2

1 BACKROUND

1.1 The aim of the test

The aim was to study how a pavement on thaw-weakened and saturated subgrade will react to wheel loads. The aim was also to study how a reinforcing steel net improves the bearing capacity of a pavement during thawing. The main interest was to test the subgrade, not surfacing. Full-scale wheel loading on a pavement on thaw, frost-susceptible subgrade was carried out in the spring of 1998 using the Heavy Vehicle Simulator (HVS-NORDIC). The subgrade was designed to freeze and thaw so that the thaw-weakening conditions would correspond to the natural state. The tested pavement was designed to fail within 2 weeks of the start of the test. Furthermore, the aim was to monitor the critical stresses, strains and deflections during loading, as well as plastic deformation via the rutting and cracks. One of three tested pavements was reinforced. The environmental conditions and test parameters were monitored and controlled before, during and after the tests.

1.2 Frost action

The damage from frost action results in ice segregation and lensing in the soil and the subsequent loss of soil strength when the ground ice thaws. Frost heave can damage road and airfield pavements (Fig. 1). In cold climates, unheated structures that have concrete or asphalt floors can also be damaged by frost heave - as well as driveways, patios, and sidewalks.

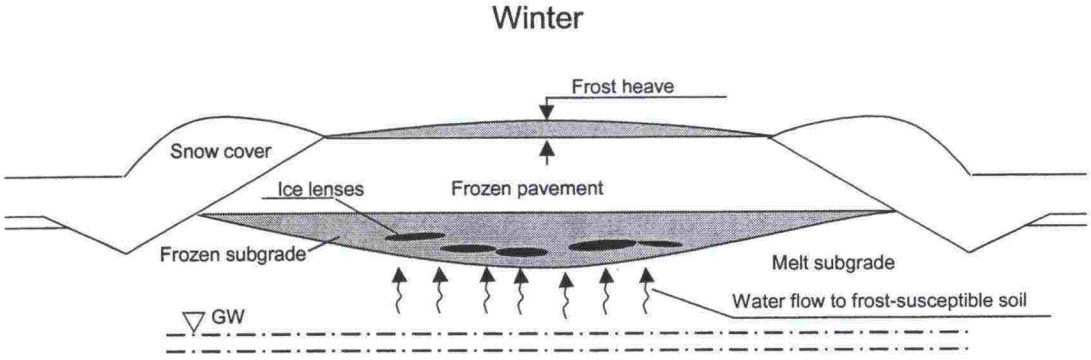

Figure 1. Frost action and frost heave in pavement.

The thawing of the ice causes settlements and produces free porewater on the still frozen soil below (Fig. 2), and the soil stiffness is reduced (Fig 3). This increases both elastic and plastic deformations under traffic loads, which may cause serious damage. In addition, the back-slopes and side-slopes of cuts and fills may slide during thawing. Silts and varved soils with a high water table in winter are the most susceptible to frost action.

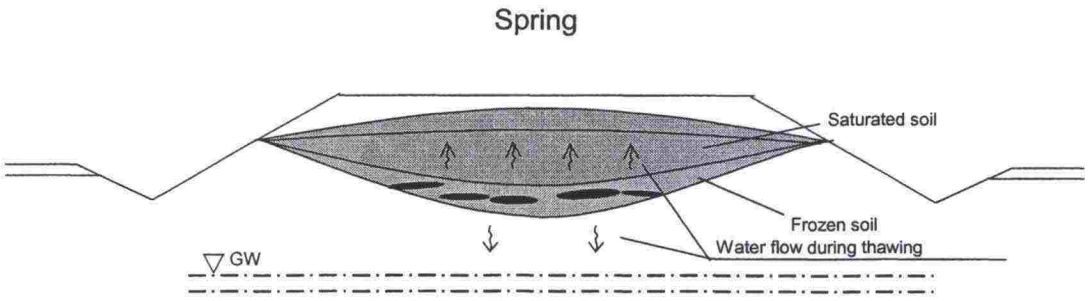

Figure 2. Thawing in pavement.

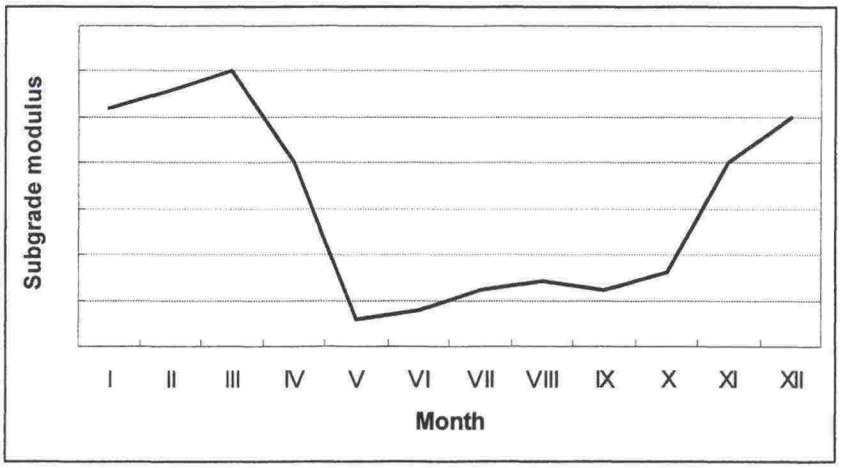

Figure 3. General view of seasonal variation of subgrade modulus in Finland.

2 TEST SITE, TESTED PAVEMENTS AND INSTRUMENTATION

2.1 Test site in Otaniemi

The test pavements can be constructed in two trough-shaped test basins. One of them is a concrete basin and the other is excavated in rock. The tested frost-susceptible pavements were made in the concrete basin. The walls of the concrete basin are thermally insulated and equipped with a complete groundwater table regulation option. Its length is 36m including a 16m-long entrance slope. Its depth is 2.5m and width 4m at the top and 3m at the bottom. There is a 3x3m part of the test basin, which is 4.5m deep for special studies. Two or three different test pavements can be constructed in a test basin.

The second test basin is parallel to the first one. It was excavated mainly in rock and it has no groundwater table regulation. It is roughly of the same size as the concrete basin.

A tent covers nearly the whole rock basin and it is large enough to house the HVS-NORDIC. Another smaller tent was temporarily used when the basin was constructed for frost-susceptible test sections (Fig. 4).

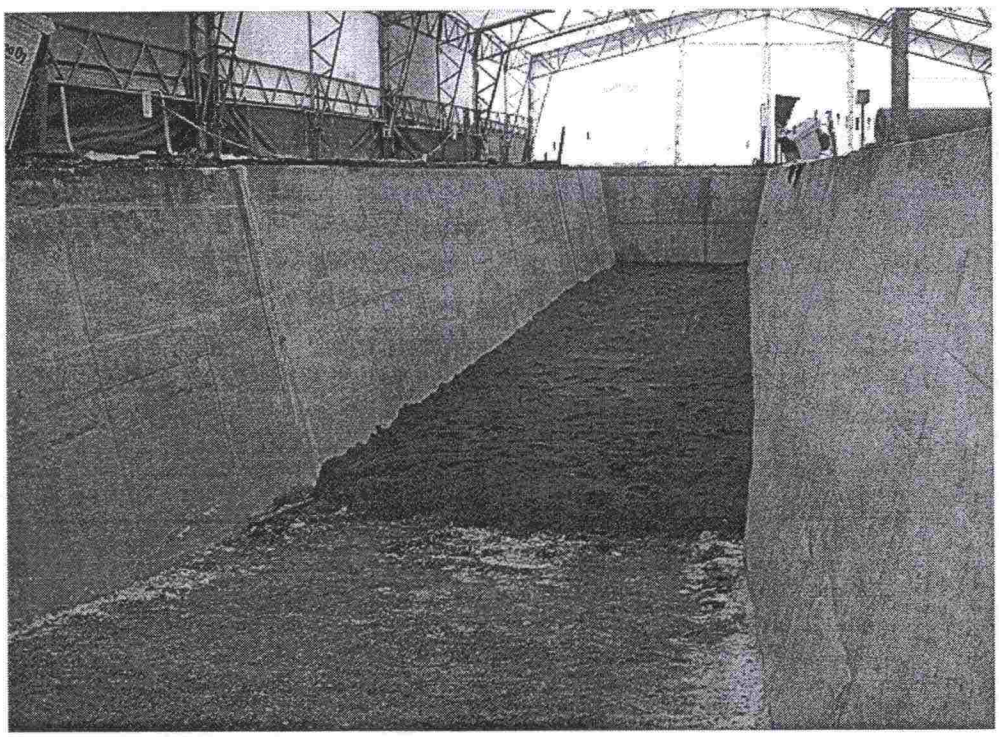

Figure 4. Concrete basin under a temporary covering tent in Otaniemi in the winter of 1997. The subgrade filter layer was compacted on the bottom of the basin.

2.2 Frost-susceptible test sections

The subgrade filter layer consisted of a 100mm gravel layer and 500mm fine sand, in which the groundwater level could be regulated. A geotextile was installed on the surface of the gravel and a composite fabric was placed on the sand surface (type Comtrac 55/30B30, operating class 3). The fabric edges were folded up along the basin side to the level of the clay surface.

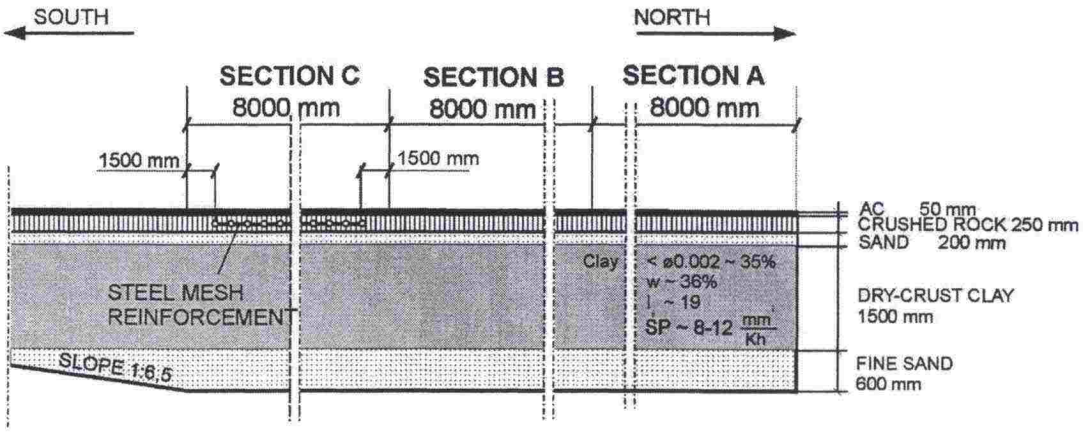

Figure 5. The longitudinal profile of test basin.

The frost-susceptible subgrade was compacted in six layers to obtain a natural density and degree of saturation. The total thickness of the clay was 1500mm. On top of clay was a composite fabric.

Three test sections consisted of a 500mm-thick pavement. The tested pavements were constructed on the frost-susceptible subgrade. The pavements consisted of a thin asphalt surfacing of 50mm, a 200mm base layer of crushed rock and a 250mm sub-base layer of sand. In one of the three sections, a reinforcing steel mesh was installed in the base layer.

After construction of the test pavements, three 8x1m loading areas were marked off on the asphalt. These areas were named Sections A, B and C (Fig. 5). The cross-sections of these pavements are illustrated in Figs. 6 and 7 (in the HVS testing programme, these sections are called test 06, 07 and 08).

After paving, the groundwater level was elevated to the clay surface in December 1997. During the following frost season, the groundwater level was lowered to the level of -1500mm from the surface. The surface of the pavement was exposed to atmospheric frost temperatures.

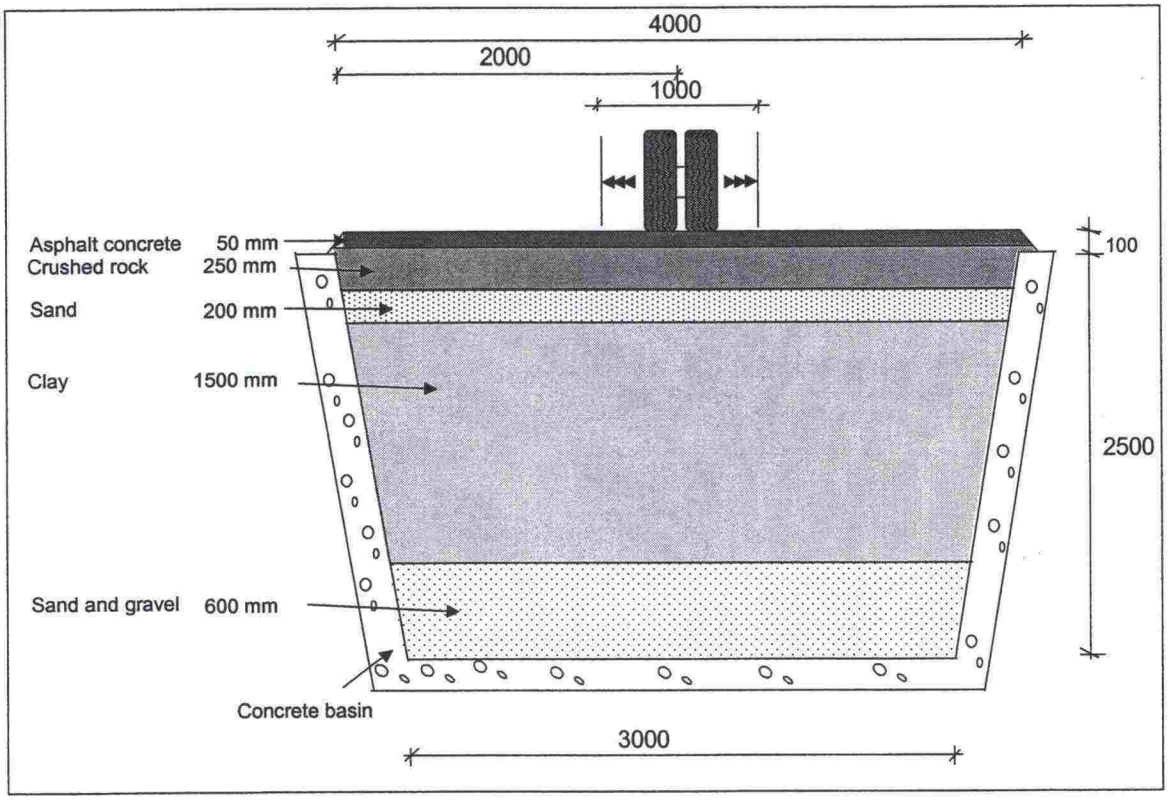

Figure 6. Sections A and B, design dimensions.

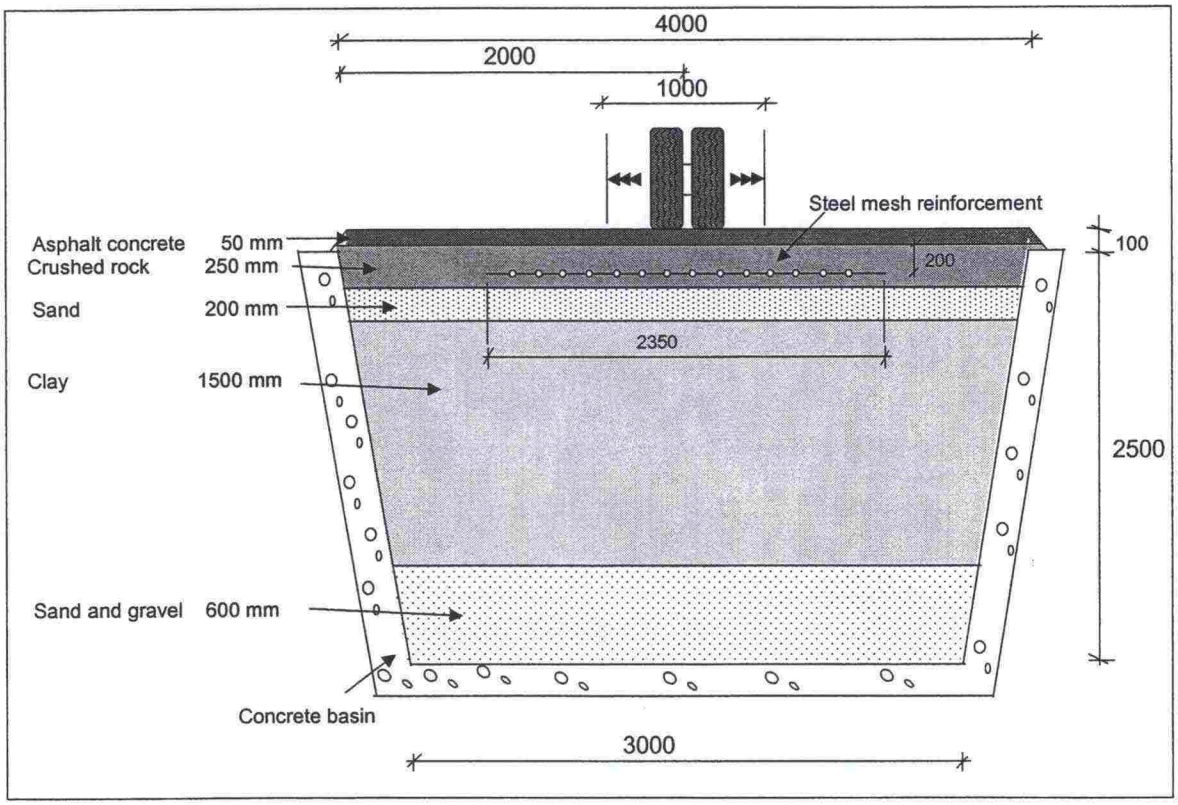

Figure 7. Section C, design dimensions.

2.3 Instrumentation

2.3.1 Purpose of instrumentation

The aim was to monitor the stresses, strains and deflections at critical locations during loading as well as the plastic deformation via the rutting and cracks. In addition, during the freeze-thaw cycle, special instruments were used to observe the temperatures, and changes in moisture and pore pressure. Some instruments were installed during the construction and some after paving.

2.3.2 Instruments installed during and after construction

Table 1 shows the different instrument-types that were installed in the pavement during construction.

Table 1. Instrumentation during construction

Measured quantity	Instrument	Number (all sections)
Water content (vol.)	Trime-EZ	3
Earth pressure	pressure cell - Nottingham - SGT - TML KD-D	 16 16 3
Bearing capacity	loading plate	12
Temperature under loading plates	thermocouple	12
Strain in steel mesh	strain gauge	23

The reinforcing steel mesh in Section C was made of a 6/6mm deformed steel bar with a 150x150mm mesh. A total of 23 strain gauges were glued to the mesh. The gauges were installed both in the longitudinal and transverse bars. The total size of the reinforcement was 2350x5000mm. The effective size of the mesh was 2250x4800mm. The net was installed about 5cm above the bottom of the base layer (Fig. 7), and positioned centrally under the loading area.

A total of 35 earth pressure cells were installed in different layers. The measuring range of the SGT and TML-type cells were 0—200kPa, and the Nottingham-type cells 0—500kPa. Eight of the earth pressure cells were in Section A, 12 in Section B and 15 in Section C. Mostly, these cells were installed to measure the vertical pressure in the subgrade layer and sand. Some of the cells also measured the horizontal pressure both in the longitudinal and transverse directions (towards the test wheel drive). The pressure cells were calibrated in the laboratory before instrumentation.

Figure 8. The mounting of instruments after paving. The edges of the 8x1m loading areas were marked with yellow paint.

The instruments installed after paving consisted of gauges to monitor frost penetration, heat flow and moisture in the structure as well as the pore pressure in the clay and strains in the asphalt (Fig 8.). Asphalt strains were measured at the bottom and on the surface of the bound layer. Retrofit strain gauges were used in the tests, which consisted of four longitudinal and four transverse gauges at the bottom, and three longitudinal and three transverse gauges on the surface of asphalt in each section. Surface deflection was measured with a fixed rod and a deflection gauge during loads. A rigid steel rod was anchored in a drill-hole to the bottom of subgrade. The deflection gauge was fixed in the asphalt with an aluminium cylinder. The instruments installed after paving are presented in Tables 2 and 3.

Table 2. Instrumentation after paving.

Measured quantity	Instrument	Number (all sections)
Atmospheric air temperature	temperature gauge	2
	thermometer	1
Asphalt temperature	copper constantan thermocouple	9
Temperature profile	copper constantan thermocouple	60
Heat flow	Heat flow gauge	1
Frost penetration	Frost tube	6
Frost heave	Levelling	>6
Pore pressure	Piezometer	6
Density and volumetric water content	Radiometric measuring tube (VPGR)	3
Groundwater	Observation tube	3
Surface deflection	Deflection gauge	2 (Sections A and C)
Asphalt strain	Strain gauges	42

Table 3. Pore pressure transducers.

Section	Depth from surface		Date of installation	Thaw penetration
A	0.60m	0.80m	23.4.1998	0.67—0.75m
B	0.65m	0.85m	6.5.1998	0.62—0.67m
C	0.63m	0.82m	25.5.1998	0.75—0.79m

In all sections, two pore-pressure transducers were installed (type Druck miniature PDCR 81) for pore-pressure monitoring. The piezometers were calibrated in the laboratory before installation. These gauges were considered to react very fast to the pressure.

3 TESTING OF FROST-SUSCEPTIBLE SECTIONS

3.1 Testing with the HVS-NORDIC

The HVS-NORDIC was manufactured in South Africa and it was financed by the Road Administrations of Sweden and Finland as well as the Technical Research Centre of Finland (VTT) and the Swedish National Road and Transport Research Institute (VTI). It is a 23m-long, 3.7m-wide and 4.2m-high facility, which weighs 46 tons (Fig. 9). The HVS is totally computer-controlled. It can be operated by diesel aggregate, or the required electricity can be taken from the power net. The diesel motor also provides power for the heating/cooling system, and the simulator is independent of external power, if necessary.

The HVS has a heating/cooling system, by which the air inside the isolation space is kept under control in order to keep the pavement temperature constant. The temperature of the pavement can be between -5 and +35°C when the outside air temperature is +25°C. During testing, the standard pavement temperature was selected to be +10°C. The HVS-NORDIC is the only mobile APT facility in the world with full temperature control.

Figure 9. The HVS-NORDIC is parked on the concrete basin in Otaniemi. A white isolation wall can be seen under the frame.

The loading is linear and can be uni- or bi-directional. The HVS-NORDIC also has a dynamic loading capability. The loading can be varied dynamically +/- 20% of static load in the sinusoidal mode. The loading wheel can be dual (max. size 2x295/65R22,5) or single (max. size 425/65R22,5). The wheel load can be selected from between 20kN to 110kN, with corresponding axle loads of 40kN to 220kN. The speed of the test wheel can be selected from 1 to 12 km/h. The length of the loading area

is 8m, where a 6m-long middle section is uniformly loaded with constant speed. The lateral movement of the loading wheel can be 0.75m with 0.05m steps (the loading beam can have 16 different lateral positions). This means that the total width of the loading area can be about 1.5m (with dual wheel). The lateral loading distribution can be arbitrary. VTT (and VTI in Sweden) uses 1m-wide test areas. It is possible to get 25 000 load repetitions per day (24h), when loading is bi-directional.

3.2 Soils testing and site measurements before testing

3.2.1 General

It was seen very important that at least one freeze-thaw period should be passed before testing. During this period, the aim was to monitor how the structure behaved under natural conditions. The frost and thaw penetration were monitored and sampling for clay was conducted. Test results are presented in Chapter 4.

3.2.2 Sampling for clay subgrade

First, the samples for laboratory testing were taken from the clay deposit in the town of Lahti (about 100km north of Helsinki). The determined parameters for natural clay were grain size distribution, consistency limits and moisture content.

Second, the clay samples were taken from the subgrade in Otaniemi during construction and after paving. The determined parameters for the Otaniemi samples were dry density, porosity, void ratio and degree of saturation corresponding to natural state. The consistency limits of the clay were also determined as well as the hydraulic conductivity.

Frost heave tests were performed for samples taken from Lahti and Otaniemi to determine the segregation potential and relative frost heave in the laboratory. During the freezing season, when frost penetration was at its maximum, two frozen samples were cored from the clay subgrade with a drill sampler. Thaw-consolidation test were done on them in the laboratory.

3.2.3 Monitoring during winter 1997-98

The asphalt surface and the tops of the frost tubes were levelled after paving. The air and surface temperatures were monitored with thermocouples. The volumetric moisture content and dry density were measured with a radiometric device at 10cm intervals using a casing tube.

The ground water surface was measured from observation tubes, and the excess pore pressure in the clay was monitored during the winter. Four vane shear soundings and two cone penetration tests were carried out to determine the shear strength of the clay.

The surface modulus of the pavement was measured during freezing and thaw using the falling weight deflectometer test (FWD), plate loading test and Loadman apparatus test. FWD measurements were also performed during construction on the base layer surface. Strain gauges were registered twice in the steel net during the FWD measurements in winter.

During freezing, the asphalt pavement was kept clear from snow to maintain the frost effect as efficiently as possible. Groundwater table was kept at a level of 1.5m below the surface.

The frost penetration and frost heave of the surface were monitored, as well as the pore-pressure development under the freezing front. The winter of 97-98 was mild in Finland, so an excess cooling of the pavement had to be applied using artificial freezing to reach the frost penetration of about 1.2 metres. The test results are presented in Chapter 4.

3.3 Wheel loading

3.3.1 Loading in different test sections

Testing with the HVS was started when the pavement had thawed to the depth of 0.80–0.90m. The sections were tested in the order A, B and C. During testing, untested sections were isolated to prevent untimely thaw. A temperature control box was installed over the tested section. The temperature in the asphalt was kept at +10°C. The wheel loading was unidirectional during all passes and the wheel was of type 2x295/65R22,5. The loaded wheel ran from south to north over the test surface and was returned unloaded.

Pre-loadings were conducted before the initial measurements and actual test loadings. The purpose was to compact the pavement to the initial state. After the pre-loading, the initial measurements (or zero measurements) were carried out. The gauge readings were registered with strain amplifiers and a data logging computer. After this, the actual test loading was started. Tables 4, 5 and 6 present summaries of the test procedure.

Table 4. Summary of Section A (test06).

Structure

50mm	AC
250mm	Crushed rock
200mm	Coarse sand
1500mm	Clay
600mm	Fine sand

Loading conditions

AC's temperatu	10°C
Test wheel	dual
Thaw depth	800 - 900mm from the surface

Schedule HVS test parameters

Date	Operation	Total no. of passes	Wheel speed km/h	Tyre press. kPa	Wheel load kN	Type of loading
24.4.1998	HVS was moved to area 06 (A)	-	-	-	-	-
27.4.1998	preparative tasks	0	-	-	-	-
28.4.1998	pre-loading	250	12	500	20	unidirectional
29.4.1998	initial measurements	596	2-10	500-700	20-50	unidirectional
30.4.1998	testing	790	12	700	50	unidirectional
30.4.1998	test ended	4881	12	700	50	unidirectional
6.5.1998	ending measurements	4952	10	700	30-50	unidirectional
6.5.1998	HVS was moved from area 6 (A)	-	-	-	-	-

In pre-loading, the applied wheel load was 20kN on the all sections. During zero measurements, the loads and tyre pressures were varied (loads 30—50kN). The lateral position of the test wheel was applied along the centreline or 15cm left, see Fig. 10. The procedure of Initial measurements was quite similar for all the sections.

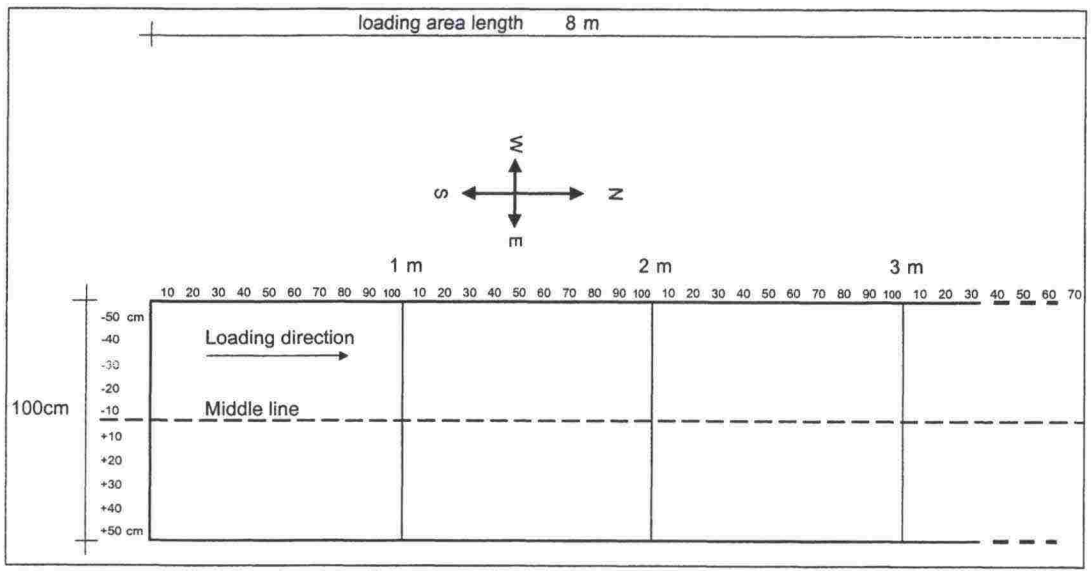

Figure 10. Plan of loading area.

Table 5. Summary of Section B (test07).

Structure

50mm	AC
250mm	Crushed rock
200mm	Coarse sand
1500mm	Clay
600mm	Fine sand

Loading conditions

AC's temperatu	10°C
Test wheel	dual
Thaw depth	800 - 900mm from the surface

Schedule

		HVS test parameters				
Date	Operation	Total no. of passes	Wheel speed km/h	Tyre press. kPa	Wheel load kN	Type of loading
7.5.1998	HVS was moved to area 07 (B)	-	-	-	-	-
8.5.1998	preparative tasks	-	-	-	-	-
11.5.1998	benkelman beam measuring	20	1	500	20-40	-
12.5.1998	pre-loading	270	12	500	20	unidirectional
12.5.1998	initial measurements	456		500	30-49	unidirectional
13.5.1998	initial measurements	648	2-10	550-700	30-50	unidirectional
14.5.1998	initial measurements	629	2-10	550-700	30-50	unidirectional
14.5.1998	testing started	768	12	550	40	unidirectional
14.5.1998	testing	1140	12	550	40	unidirectional
14.5.1998	testing	1256	12	550	40	unidirectional
14.5.1998	testing	1600	12	550	40	unidirectional
14.5.1998	testing	2000	12	550	40	unidirectional
14.5.1998	testing	2104	12	550	40	unidirectional
15.5.1998	testing	2104	12	550		unidirectional
15.5.1998	benkelman beam measuring	2130	1	550	20-40	-
15.5.1998	testing	2500	12	550	40	unidirectional
15.5.1998	testing	2602	12	550	40	unidirectional
15.5.1998	testing	3000	12	550	40	unidirectional
18.5.1998	testing	3500	12	550	40	unidirectional
18.5.1998	testing	4000	12	550	40	unidirectional
18.5.1998	testing	4500	12	550	40	unidirectional
18.5.1998	testing	5000	12	550	40	unidirectional
18.5.1998	testing	6000	12	550	40	unidirectional
19.5.1998	testing	7000	12	550	40	unidirectional
19.5.1998	testing	8000	12	550	40	unidirectional
19.5.1998	test ended	8111	12	550	40	unidirectional
19.5.1998	HVS was moved from area 7 (B)	-	-	-	-	-

Table 6. Summary of Section C (test08).

Structure

50mm	AC
250mm	Crushed rock + steel mesh reinforcement
200mm	Coarse sand
1500mm	Clay
600mm	Fine sand

Loading conditions

AC's temperatu	10°C
Test wheel	dual
Thaw depth	800 - 900mm from the surface

Schedule HVS test parameters

Date	Operation	Total no. of passes	Wheel speed km/h	Tyre press. kPa	Wheel load kN	Type of loading
19.5.1998	HVS was moved to area 08 (C)	-	-	-	-	-
26.5.1998	preparative tasks	0	-	-	-	-
26.5.1998	benkelman beam measuring	220	12	500	20	unidirectional
27.5.1998	pre-loading	240	1	500	20-40	-
27.5.1998	initial measurements	255	2-10	500-700	30-50	unidirectional
28.5.1998	testing started	1035	12	550	40	unidirectional
28.5.1998	testing	1035	12	550	40	unidirectional
28.5.1998	testing	1500	12	550	40	unidirectional
28.5.1998	testing	2000	12	550	40	unidirectional
29.5.1998	testing	2000	12	550	40	unidirectional
29.5.1998	testing	2500	12	550	40	unidirectional
29.5.1998	testing	3000	12	550	40	unidirectional
29.5.1998	testing	3500	12	550	40	unidirectional
1.6.1998	testing	4000	12	550	40	unidirectional
1.6.1998	testing	4500	12	550	40	unidirectional
2.6.1998	testing	5500	12	550	40	unidirectional
2.6.1998	testing	5900	12	550	40	unidirectional
3.6.1998	testing	5900	12	550	40	unidirectional
3.6.1998	benkelman beam measuring	6190	1	500	20-40	-
3.6.1998	test ended	6538	12	550	40	unidirectional
3.6.1998	HVS was moved from area 8 (C)	-	-	-	-	-

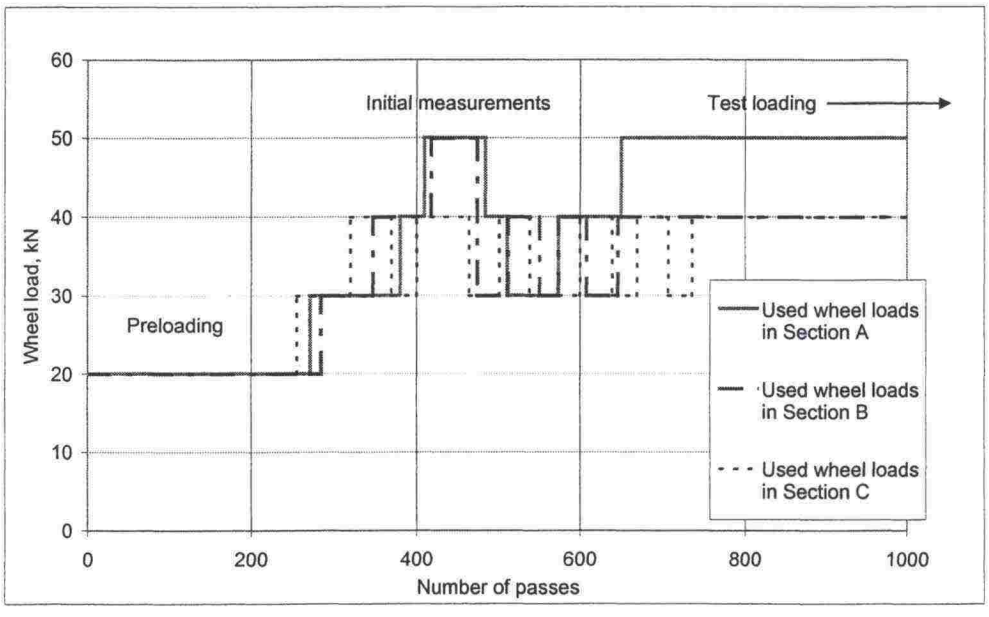

Figure 11. Applied loads (with dual wheel) during different test phases.

Testing was started with a 50kN load in loading Section A. The applied load proved to be heavy in relation to the soft subgrade, and the pavement rutted more than expected. Hence, it was decided to test Sections B and C using the 40kN wheel load. The applied loads during the tests are presented in Fig. 11.

The variations of the test wheel lateral position during pre-loading and test loading are illustrated in Fig. 12.

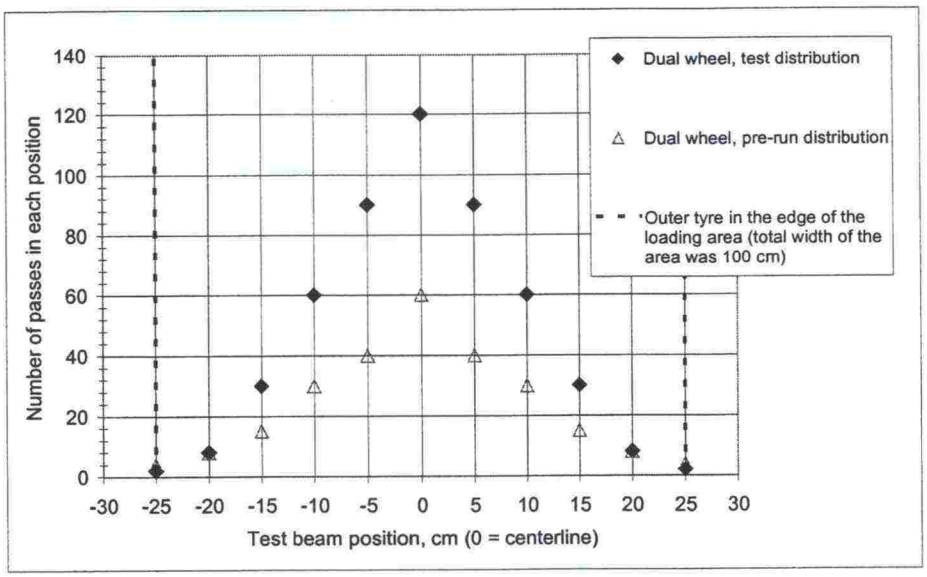

Figure 12. Number of repetitions in different test wheel lateral positions during pre-loading and testing. In testing, the number of repetitions at the centreline was 120 passes.

Figure 13. Seriously rutted test section under the moving wheel.

3.3.2 Wheel response measurements during tests

The measured response was the strain in the asphalt and steel mesh, the deflection on the surface, the earth pressure in the sand and clay, and the pore pressure in the thawed clay. Because Section A failed so early, only initial measurements could be carried out on this section.

In the response measurements, the levels were monitored and registered under the moving wheel. Signal levels were set at zero before the loading started. At the same time the overpass started, signals started to be registered too. The frequency of logging was dense (normally 250 1/s). Because the response measure system could only give results of short-term deviation from the base level, the long-term background level of the pore pressure was measured in a different manner. Test results are presented in Chapter 4.

3.3.3 Other observations

When additional rutting or cracking was detected, the rut depth was measured with a Swedish (VTI) laser profilometer (Fig. 14). Rutting was measured at one-metre intervals, and the cracks were mapped as well. Benkelman beam measurements were conducted on Sections B and C.

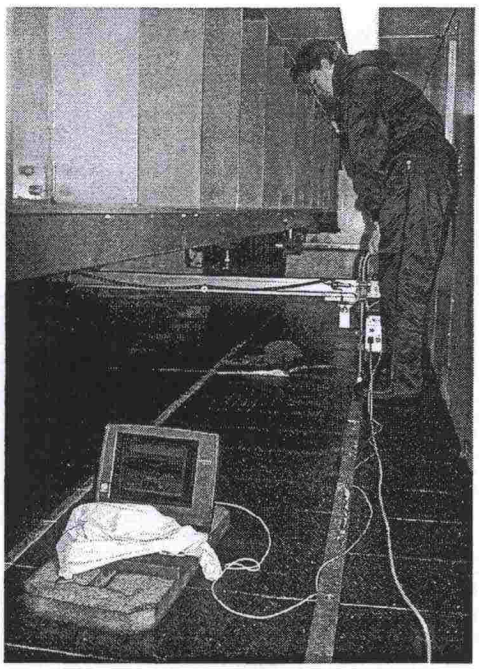

Figure 14. Rut depth was measured with a laser profilometer.

After testing, the sections were levelled and FWD measurements were carried out. The actual positions of the different layers were determined from transverse-cut profiles. They were excavated in all the sections in the summer of 1998.

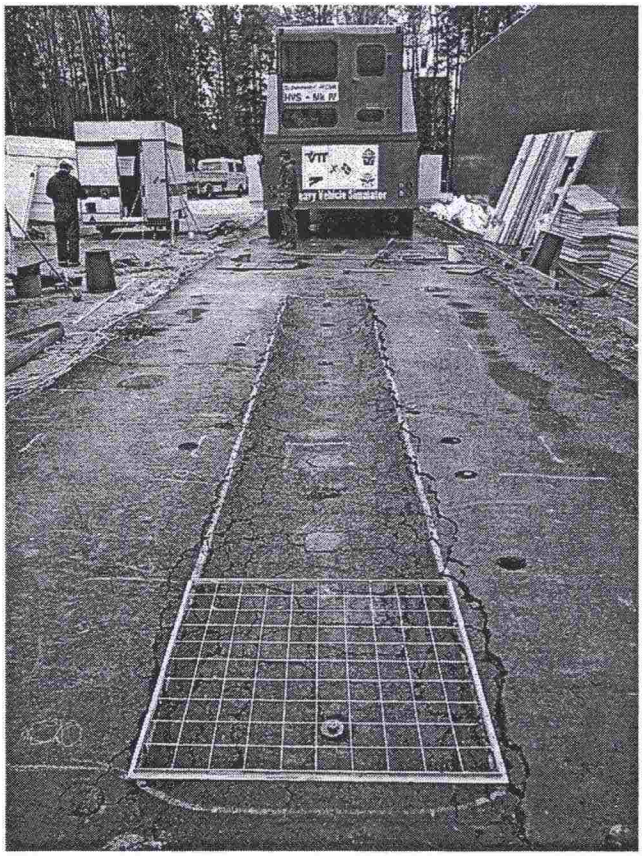

Figure 15. Rutted Section A after testing. Mapping frame in the foreground was 1x1m. The HVS-NORDIC can be seen in the background.

4 RESULTS

4.1 Laboratory investigations of the subgrade

The subgrade soil properties are presented in Table 7. Samples were taken during different construction stages. Specimen no. 8547 was taken from the truck load during transport. This clay load was compacted to the same layer as specimen no. 8549, which was drilled from the compacted structure. The layer was about 25 cm from the surface of the subgrade. According to these results, the differences in properties between natural clay and compacted clay are quite small.

Table 7. Laboratory results for the clay.

Specimen	Lab.no.	γ kN/m³	γ_d kN/m³	n %	e -	w w-%	w_{vol} vol-%
Natural clay, Lahti	8536	18.2	13.0	51.9	1.078	39.4	52.4
Sample, truck load	8547	18.7	13.8	49.1	0.963	35.8	50.3
Sample, compacted layer	8549	18.1	13.3	50.8	1.034	35.9	-

Specimen	Lab.no.	Hu %	w_l %	w_p %	I_p	S_r %	s_k kPa
Natural clay, Lahti	8536	-	-	-	-	101.0	-
Sample, truck load	8547	-	-	-	-	102.5	-
Sample, compacted layer	8549	0.50	43.5	24.5	19	95.8	96.1 - 103

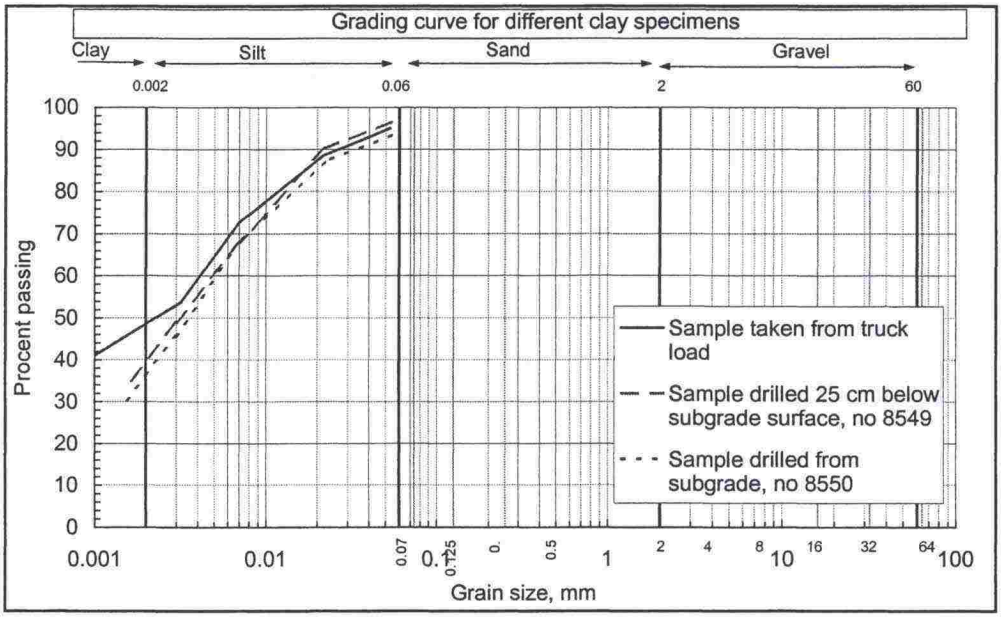

Figure 16. Grain size distribution of clay specimens.

The grain size distributions for the different specimens are presented in Fig. 16. One sample was taken from the truck load, and sample numbers 8549 and 8550 were taken from the compacted subgrade (second and top layer of the clay).

Frost heave tests were conducted on the specimens that were taken from the natural deposit and from the compacted subgrade. The determined SP values for both specimens with different surface loads are presented in Table 8.

Table 8. Segregation potentials from laboratory testing.

Applied loading	SEGREGATION POTENTIAL mm^2/Kh	
	Natural clay, Lahti	Compacted layer (no. 8549)
2 kPa	6.5 — 8.5	8 — 12
20 kPa	5 — 7.5	5 — 7
40 kPa	4.5 — 6.5	6 — 8

4.2 Freezing and thawing

Frost penetration was monitored from six methylene-blue frost tubes (two tubes per section). The total freezing index for all the sections was about 7815Kh. This value also included the estimated effect of artificial cooling.

The frost penetration was deepest after artificial cooling in April 1998. At the same time, the measured frost heave was also highest. The frost heave did not cause detectable damage to the structure. Before testing, Section A was thawed with heating fabric to reach adequate thaw depth in clay. The frost and thaw penetration is illustrated in Figures 17 to 19, as well as the frost heave and thaw settlement. The maximum frost heave was 35—50mm. The negative pore pressure was about 20—30kPa during active freezing. According to the observations, it is evident that frost heave caused a permanent compression of the frozen layer. Thus, a more realistic estimate for frost heave is the thaw settlement.

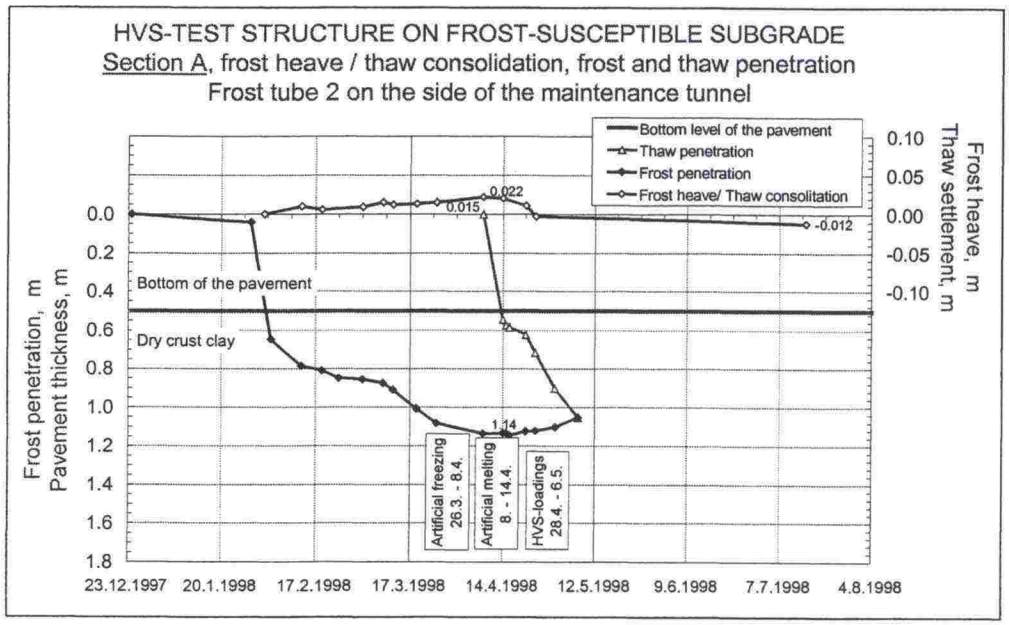

Figure 17. Section A, frost and thaw penetration as well as frost heave and thaw settlement during the winter and spring of 1998.

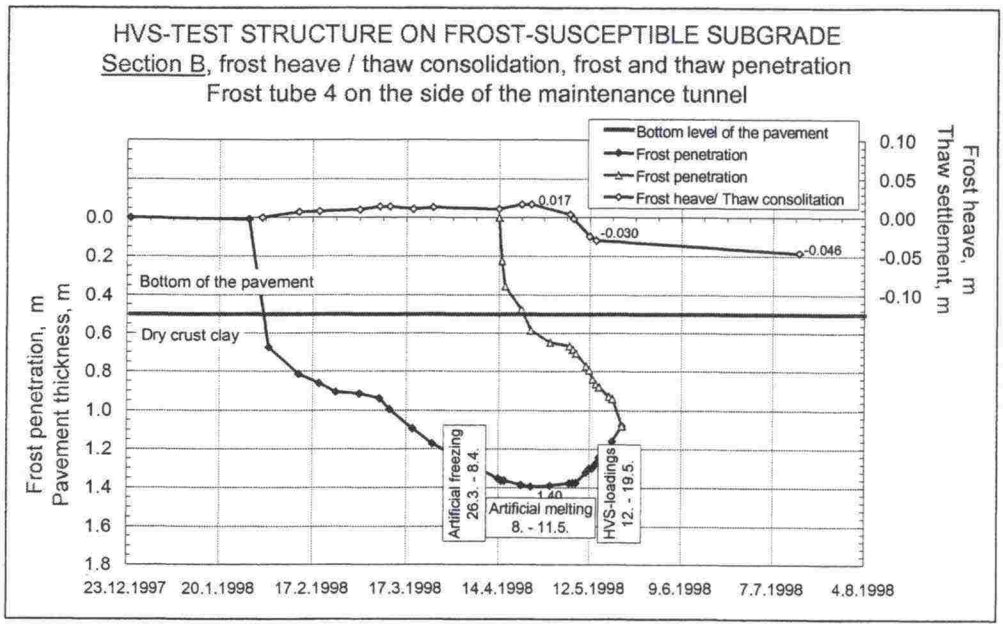

Figure 18. Section B, frost and thaw penetration as well as frost heave and thaw settlement during the winter and spring of 1998.

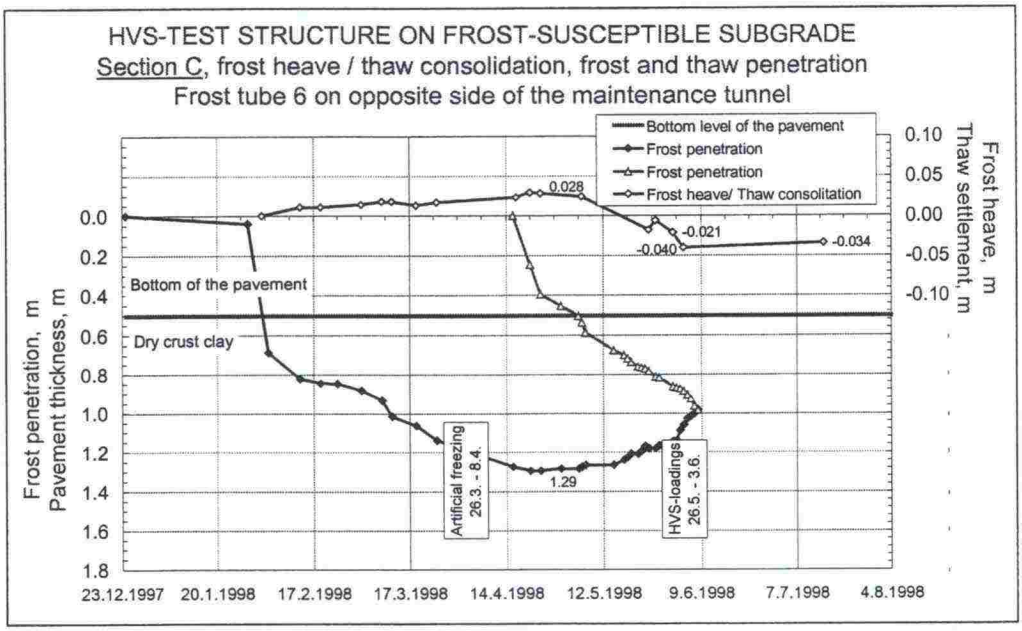

Figure 19. Section C, frost and thaw penetration as well as frost heave and thaw settlement during the winter and spring of 1998.

Frost heave was also monitored during the winter of 1998-99.

4.3 Thickness of layers in tested sections after testing

Transverse cuts were excavated in different sections to determine the actual thickness of the layers after testing. Cuts were extended down to the surface of the clay. The measured thicknesses of the layers are illustrated in Figures 20 –to 25. The figures also include estimates for layer boundaries before testing. The initial layer boundaries could not be determined accurately. It is evident that permanent deformations due to the wheel loading occurred mostly in the soft subgrade. In Figures 20 to 25 the unevenness in layer surfaces can also be seen, which was mostly caused during construction. The loaded areas are within 1.5—2.5m in the x-axis.

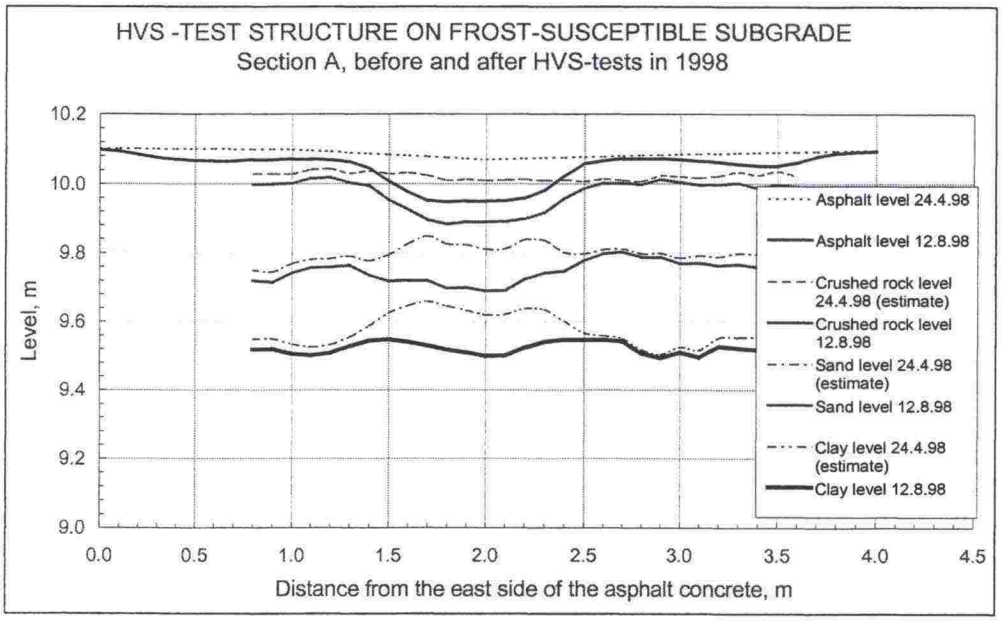

Figure 20. Cross-section of Section A. Dashed lines for unbound layers are estimates for initial levels.

Figure 21. Exposed cut face of Section A.

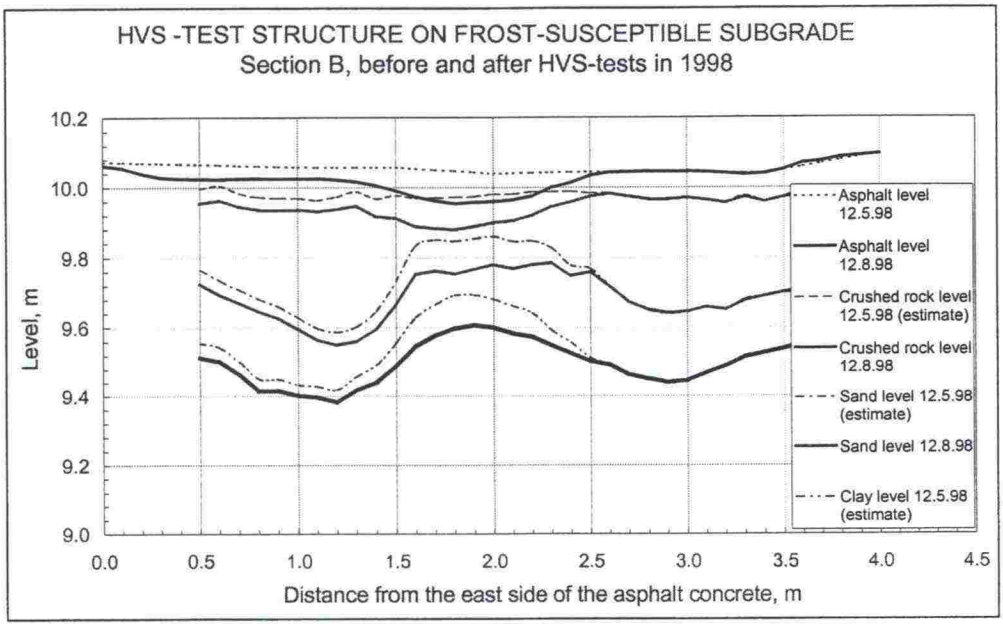

Figure 22. Cross-section of Section B. Dashed lines for unbound layers are estimates for initial levels.

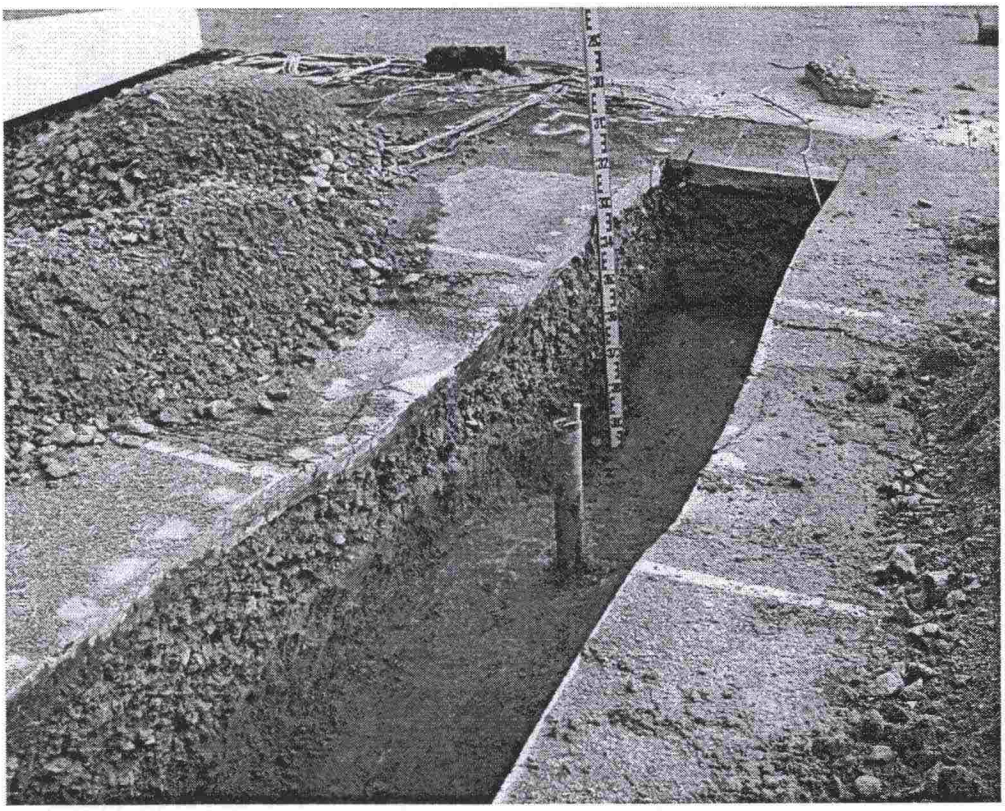

Figure 23. Exposed cut face of Section B.

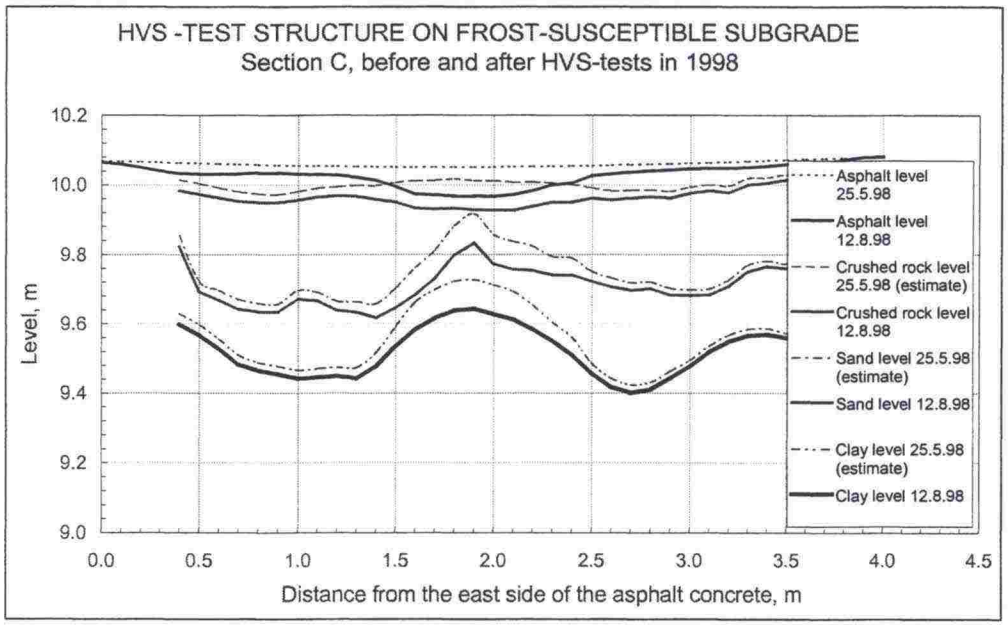

Figure 24. Cross-section of Section C. Unevenness of sublayer can be seen very clearly. Dashed lines for unbound layers are estimates for initial levels.

Figure 25. Cut face of Section C. Exposed steel mesh can be seen in crushed rock layer.

A summary of the average thicknesses of the layers is presented in Table 9. The Table includes the thaw state of clay during the FWD measurement made before testing as well as the state during testing.

Table 9. Average thickness of layers [mm].*

Layer	Section A		Section B		Section C	
	FWD 16.4.1998	Test start 29.4.1998	FWD 7.5.1998	Test start 13.5.1998	FWD 6.5.1998	Test start 27.5.1998
Asphalt concrete	60	60	60	60	50	50
Crushed rock	200	200	150	150	180	180
Sand	190	190	195	195	160	160
Thawed clay	150	450	210	448	180	420
Frozen clay	450	200	680	350	740	320
Unfrozen clay	950	900	705	797	690	870
total thickness	2000	2000	2000	2000	2000	2000

* average thickness of layers was measured after tests.

4.4 Surface modulus of test sections

4.4.1 Seasonal variation of surface modulus

The variation of surface modulus was measured using FWD (Dynatest M8000) during the freeze-thaw cycle. The measurements were carried out along the centreline on the load areas. Deflections were measured at 1m intervals.

The measured (average) surface moduli for the different sections during freezing and thawing are illustrated in Fig. 26. The surface modulus can be seen to decrease in different sections at different times. This results from the delayed thawing in later tested sections.

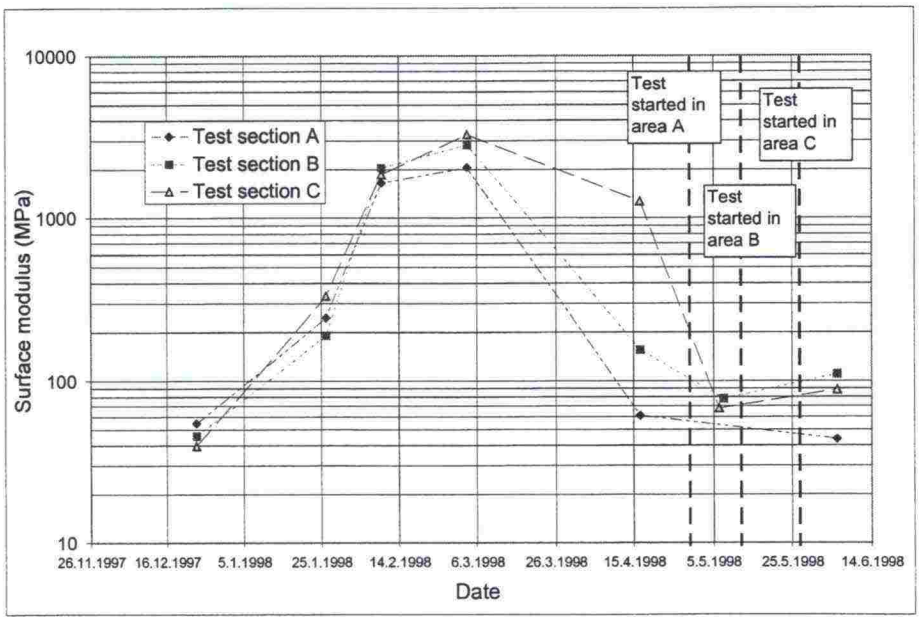

Figure 26. Measured FWD surface modulus on test sections.

The surface moduli started to decrease when the frozen soil began to thaw. The moduli were at the lowest when the subgrade was totally thawed and before post-consolidation. An interesting observation was that on Section C, a higher surface modulus could not be observed before the test, although the pavement was reinforced with steel mesh.

4.4.2 Measurements of surface deflection during testing

It was practically impossible to measure with FWD when the HVS was parked on the section. Thus, a Benkelman beam was used in Sections B and C, and a deflection gauge in Sections A and C. The gauge readings were logged during the initial measurements. A Benkelman beam was also used for rutted pavements on Section B when the number of passes was 1 600, and on C when the number of passes was 5 692). The deflection gauge functioned only on unrutted pavement. After strong rutting, the measuring range was exceeded. The applied load with the Benkelman beam was 20, 30 and 40kN. A normal test load should have been 50kN, but this was considered to be too heavy for these pavements. The test results are presented in Table 10.

Table 10. Measured deflection and estimated surface modulus during tests.

		Deflection (load 40kN), mm	Estimated surface modulus, MPa	Date
Section A	FWD	-	61	16.4.1998 *
	Benkelman	-	-	-
	Defl. gauge.	3.36	38	29.4.1998 (init. meas.)
Section B	FWD	-	78	7.5.1998 *
	Benkelman	3.96	32	11.5.1998 (init. meas.)
	"	5.74	15	15.5.1998 (N= 1600)
	Defl. gauge	-	-	-
Section C	FWD	-	68	6.5.1998 *
	Benkelman	2.95	43	27.5.1998 (init. meas.)
	"	7.30	16	3.6.1998 (N= 5692)
	Defl. gauge	1.85	69	27.5.1998 (init. meas.)

* Date is before testing and thaw penetration was then smaller than during testing. see Table 9.

According to Table 10, the measured deflection was lower under the moving wheel (deflection gauge reading) than under static loading (Benkelman beam) in Section C. If the deflection gauge results are compared between Sections A and C, it can be seen that the deflection was 40—45 % lower on Section C than on Section A. The test parameters and thaw penetration were quite similar. The only difference was that Section C was reinforced. In this case, the steel fabric seemed to resist deformations better under a moving load. The Benkelman beam measurements were not made in Section A, and therefore deflections under static and moving load could not be compared here. During the FWD measurements, presented in Table 10, the asphalt temperature was +3°C in Section A and +5°C in Sections B and

C. The Benkelman and gauge deflections were measured at a temperature of +10°C. The temperature correlation was not made for deflections.

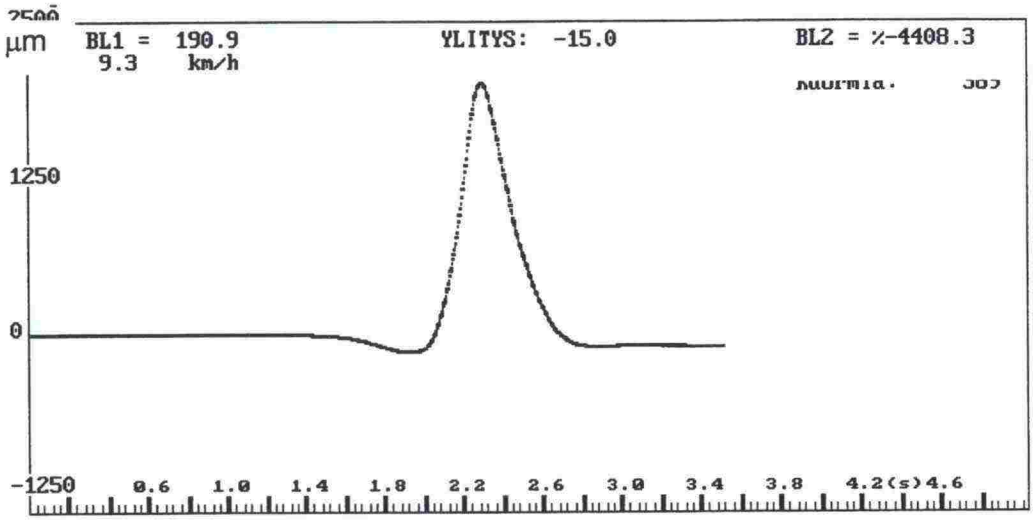

Figure 27. Deflection under moving wheel in Section C. The wheel load was 30kN during measuring.

Fig. 27 presents a deflection signal in Section C. According to the curve, the surface had slightly heaved before compressive deflection. The surface returned to the original level after loading.

4.5 Earth pressures under wheel load

An example of the earth pressure gauge signal under applied wheel load is presented in Fig. 28. The gauge readings were logged with the same response measuring system as other transient responses. In Section A, an example of the measured peak values is presented in Fig. 29.

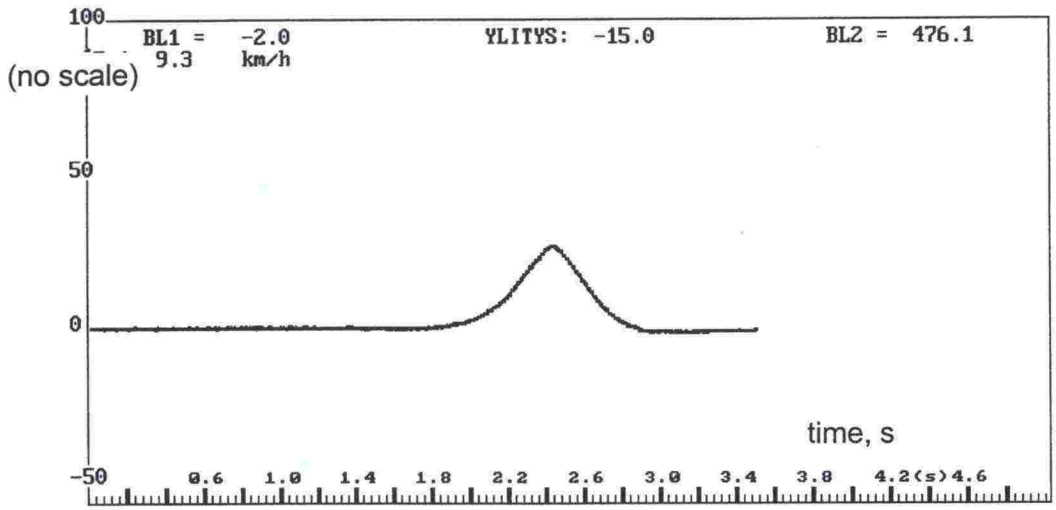

Figure 28. Example of vertical excess earth pressure signal under moving wheel load.

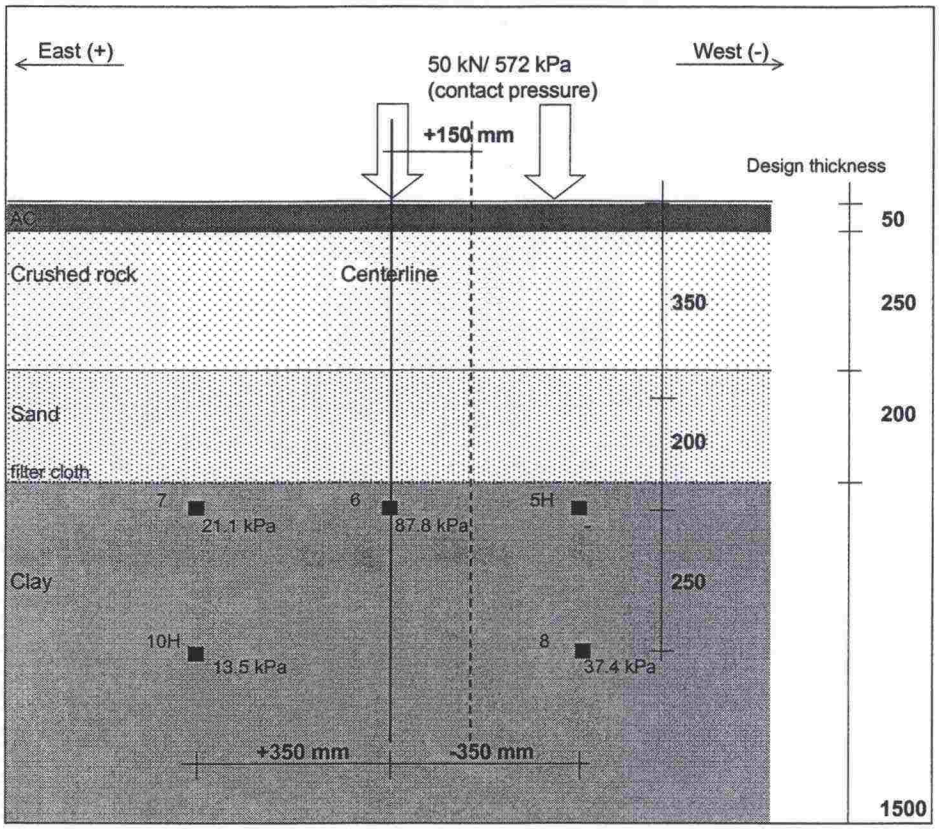

Figure 29. Section A, measured peak values for excess earth pressure. Black dots illustrate pressure cells. Sensor labels are in the upper left corner and peak values are in lower right corner of box.

The measured peak values of excess earth pressure in different sections are presented in Figs. 30 to 36. The total earth pressure was not measured, but can be estimated from the depth position of the gauges. In addition, the measured peak values at different lateral positions of the wheel are presented. The positions were relative to the longitudinal centreline of the test section. The relative positions of the pressure cells with similar coordinates are given in the legend boxes. It can be seen that the highest values were logged when the test-wheel lateral position was the same as the position of the cell, in other words, when the wheel was closest to the cell. When the test sections were rutted, some increases could be seen in pressure levels.

The presented gauge positions are 'design positions'. Some reading values are high considering the supposed gauge position and depth. The actual positions will be checked later, when the sections are opened. The calibrations will also be checked. It is possible that some types of pressure cells indicated too high readings when they were positioned in a very soft soil.

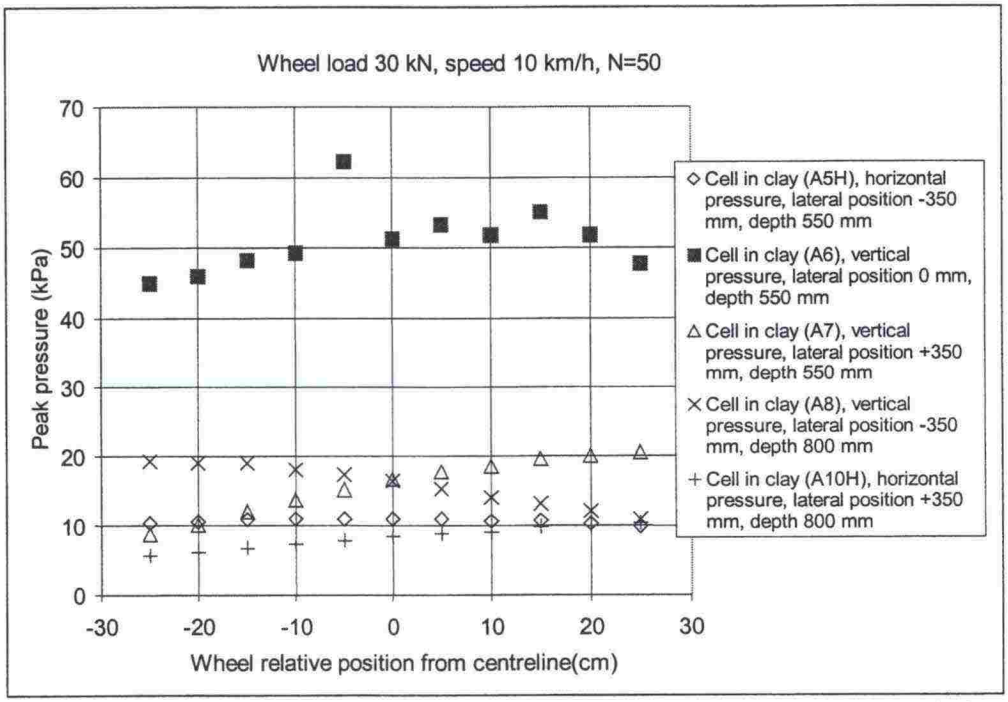

Figure 30. Section A, measured peak values of excess earth pressure during initial measurements.

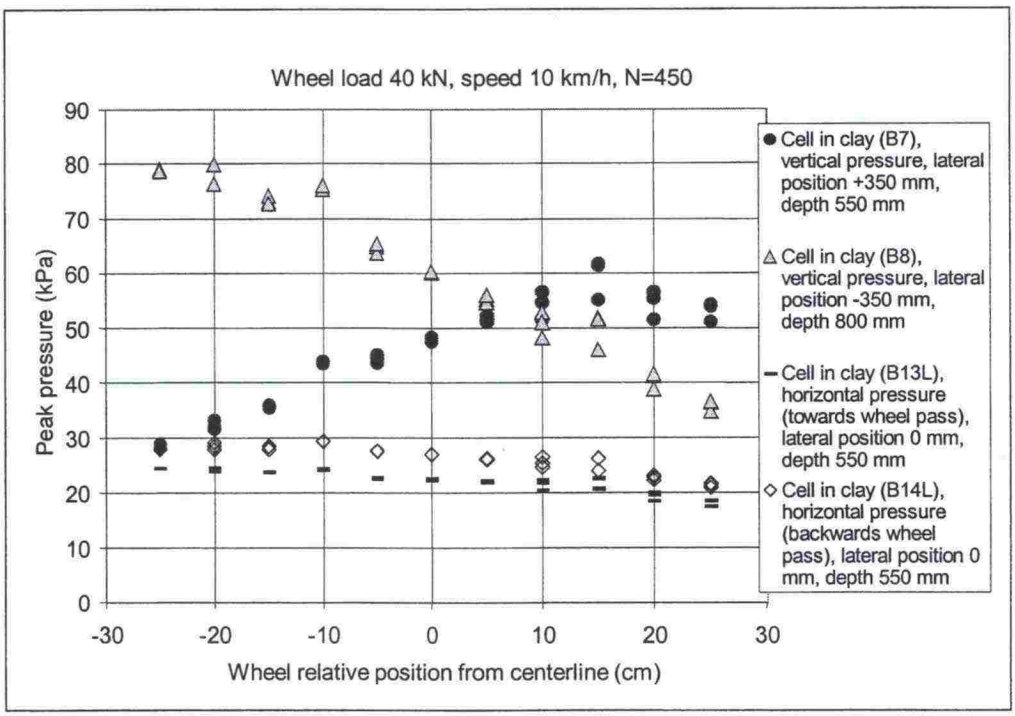

Figure 31. Section B, measured peak values of excess earth pressure during initial measurements.

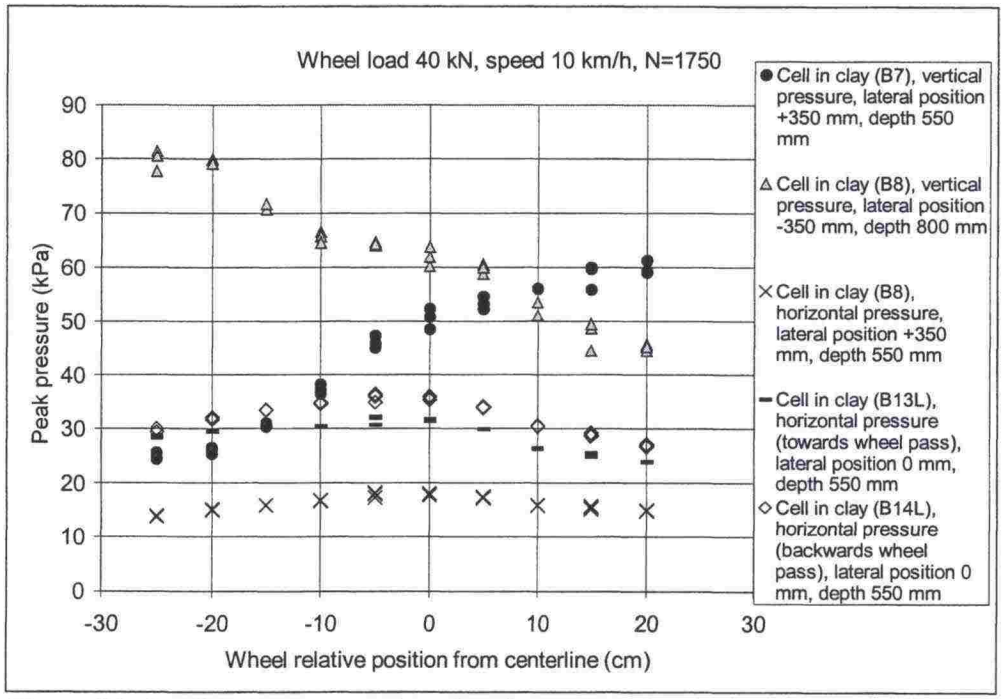

Figure 32. Section B, measured peak values of earth pressure.

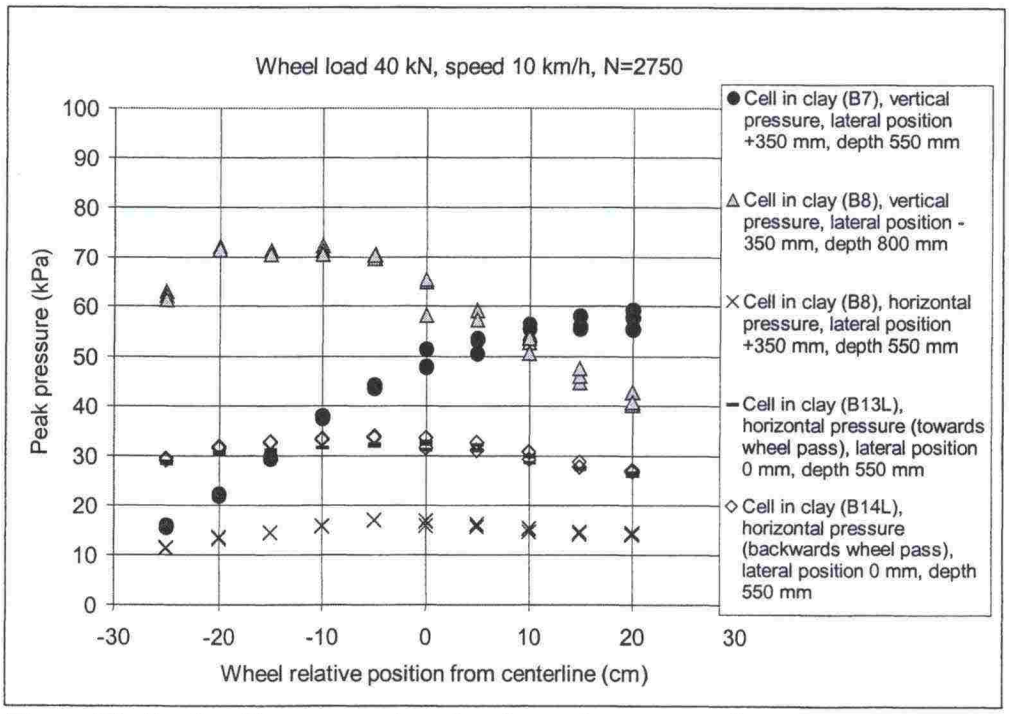

Figure 33. Section B, measured peak values of excess earth pressure.

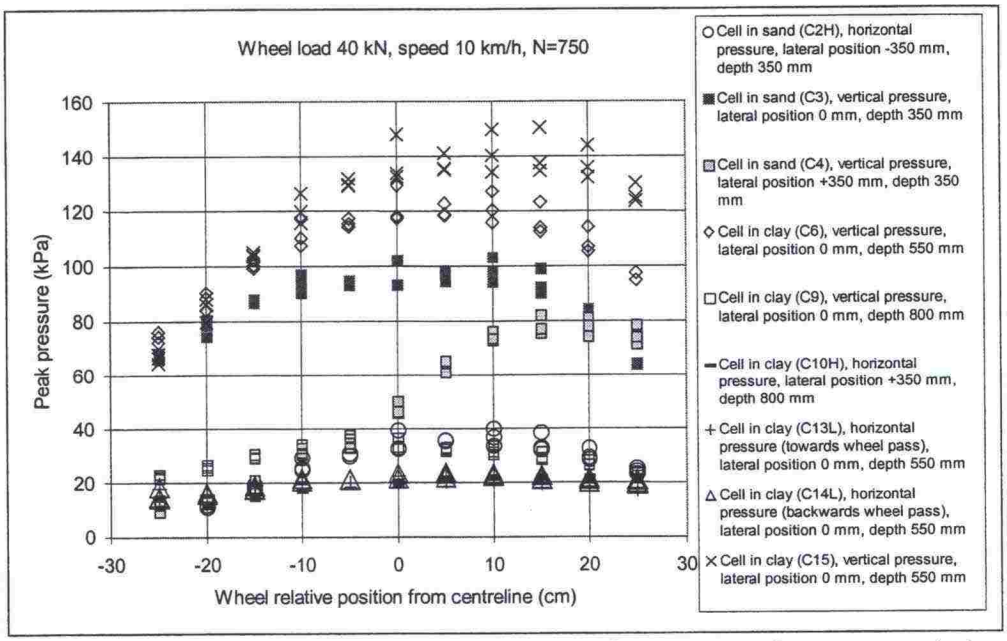

Figure 34. Section C, measured peak values of excess earth pressure during initial measurements.

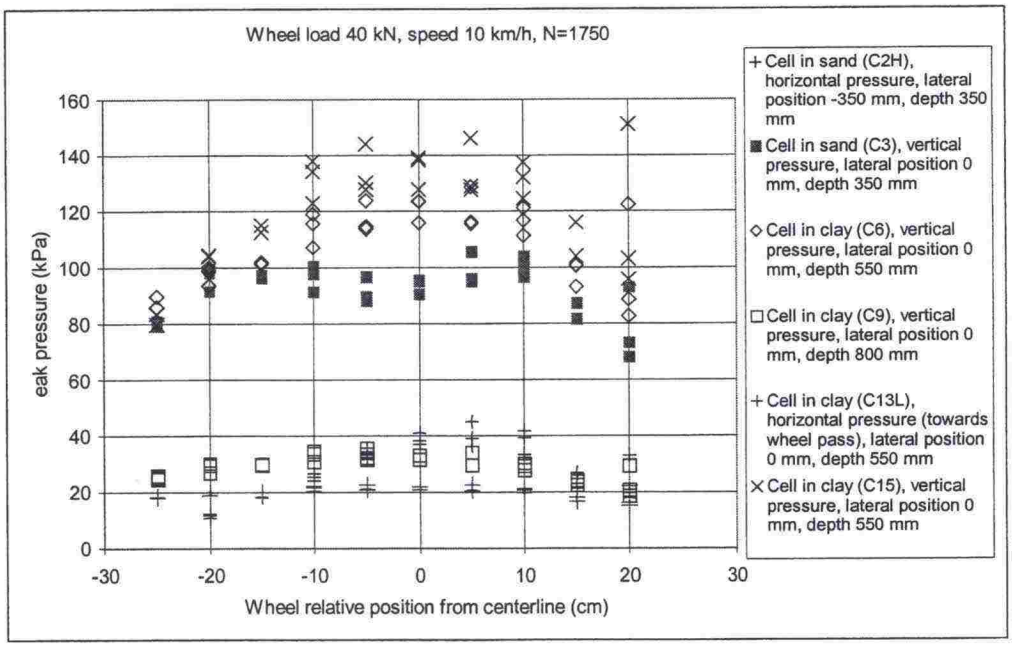

Figure 35. Section C, measured peak values of earth excess earth pressure.

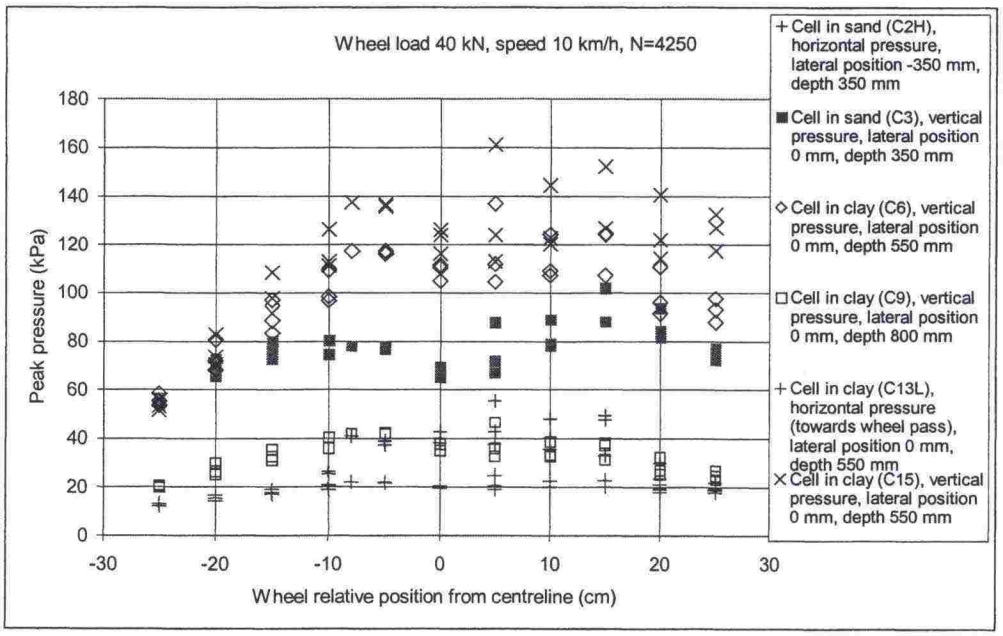

Figure 36. Section C, measured peak values of excess earth pressure.

4.6 Pore pressure in thawed subgrade

4.6.1 Long-term measurements

Long-term measurements were carried out to monitor the level of pore pressure in thawed clay. The pore pressure development in different sections during thawing and testing is illustrated in Figs. 37 to 39. Special events during test the procedure are indicated with vertical dashed lines. Excess pore pressure could be seen when the applied surface load was focused on the pavement.

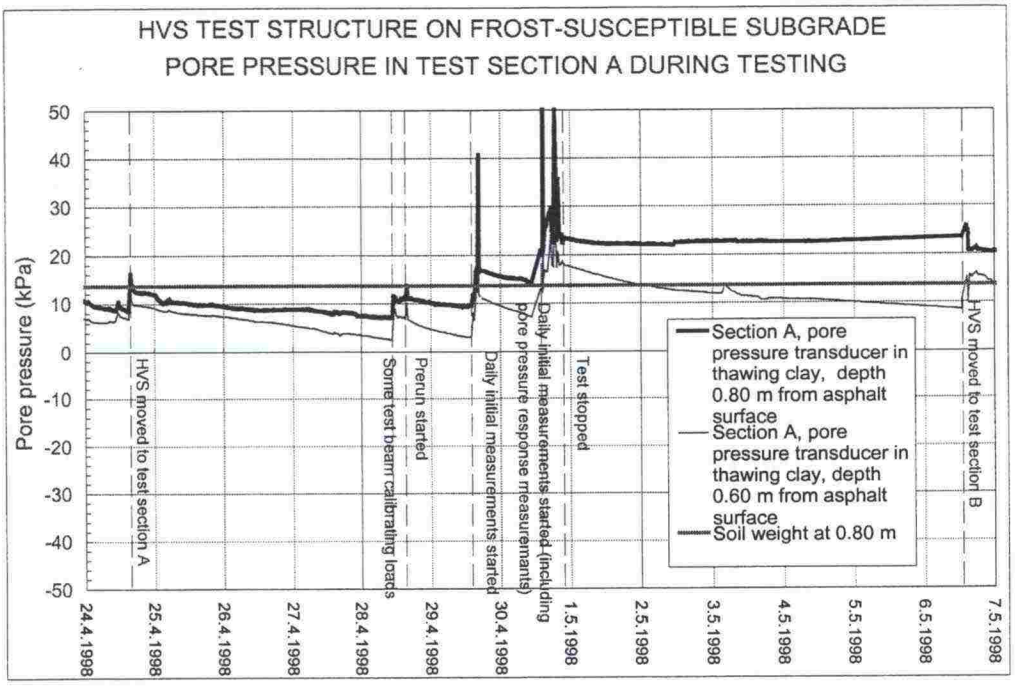

Figure 37. Section A, pore pressure development during the testing.

It could be seen that the pore pressure was higher after a period of cyclic loading than before loading. The time between two passes was about 7 seconds. It was evident that, during frequent cyclic loading, water could not discharge fast enough from the clay. Thus, the induced permanent shear deformation in the clay caused increasing pore pressure.

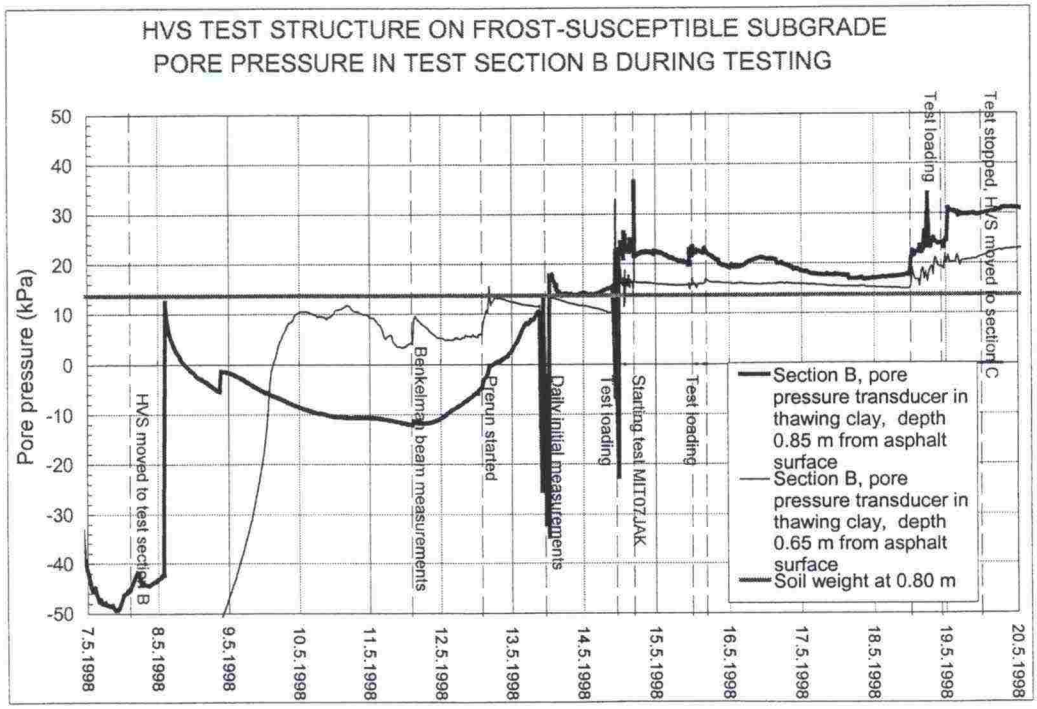

Figure 38. Section B, pore pressure development during the testing.

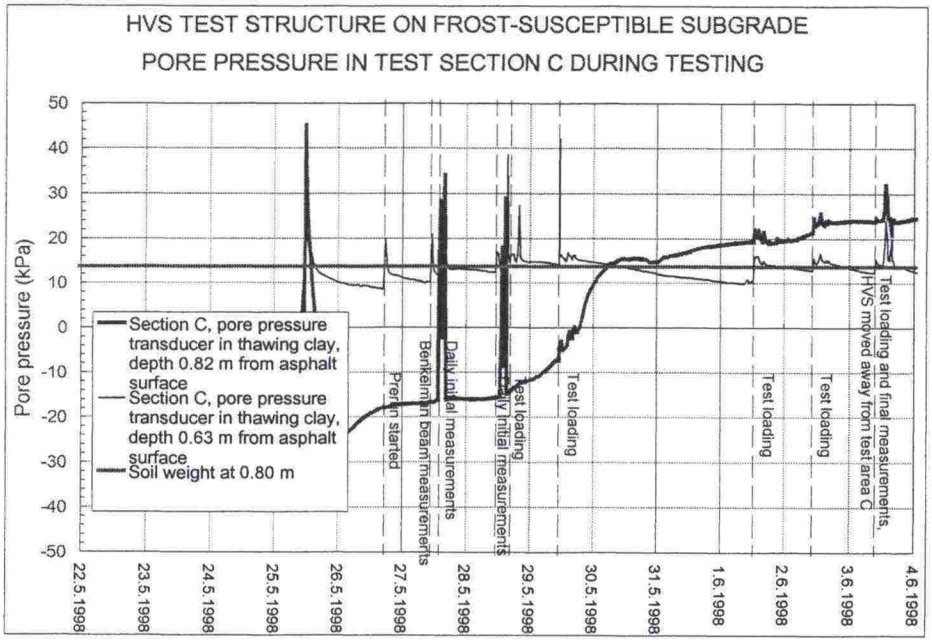

Figure 39. Section C, pore pressure development during the testing. A deeper gauge (0.82m) was inserted in the frozen clay at an early part of the test.

4.6.2 Transient pore pressure

An example of the pore pressure gauge signal under applied wheel load is presented in Fig. 40. When the test wheel was moved, this caused a fast stress pulse in the pavement. This developed a transient pore press increment under undrained conditions in the saturated clay. Excess pore pressure may have reduced the shearing resistance and stiffness of the clay. The measured peak values are presented with the modelling in Chapter 5.2.2.

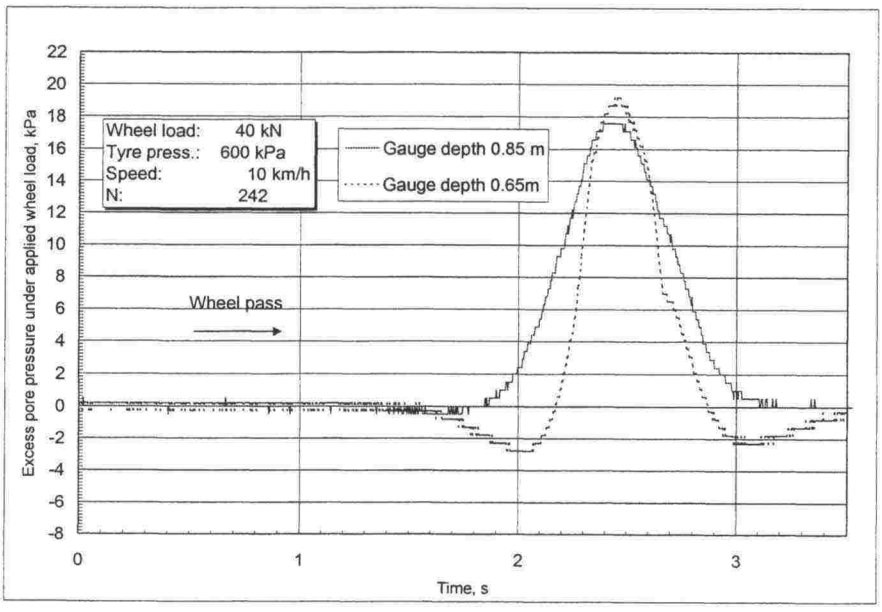

Figure 40. Section B, excess pore pressure under moving test wheel in thawed clay.

4.7 Strains in the steel net

An example of the logged signal under the wheel overpass (code H3L) in the steel bar is presented in Fig. 41. This strain gauge was installed longitudinally on the steel bar side. The applied wheel load was 40kN, and the positive values were tension and negative compression.

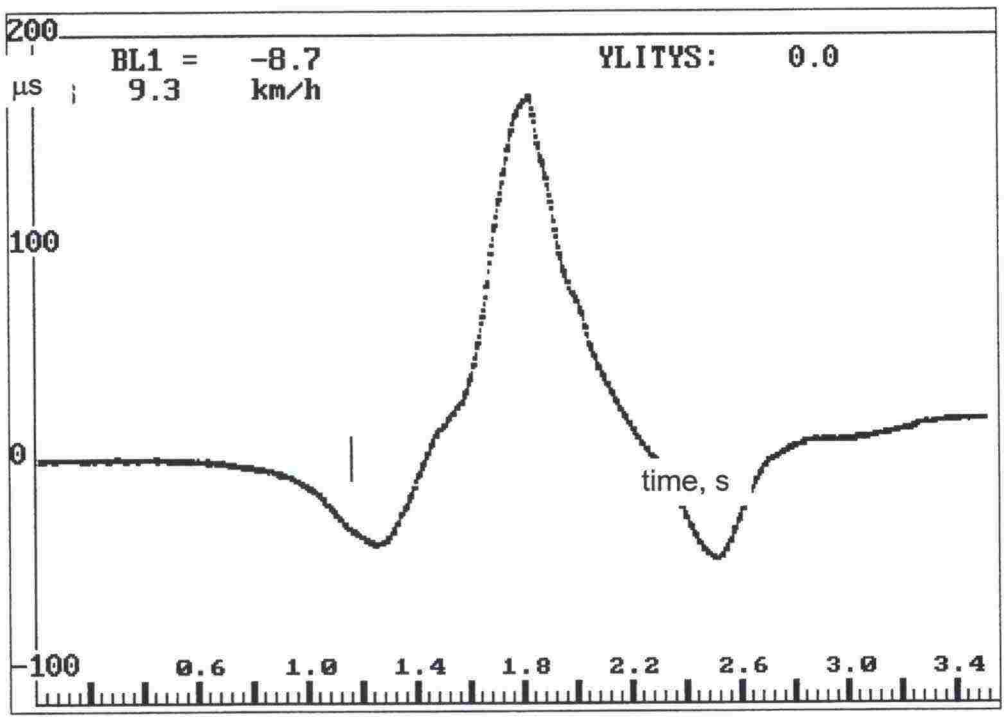

Figure 41.Section C, strain in a steel bar under the moving wheel. The applied wheel load was 40kN.

The locations of the logged strain gauges are illustrated in Figure 42. The response in the steel net was measured under the applied wheel. Some readings were logged also under FWD loading during freezing. During the FWD loading, the loading plate was placed centrally above the logged gauge.

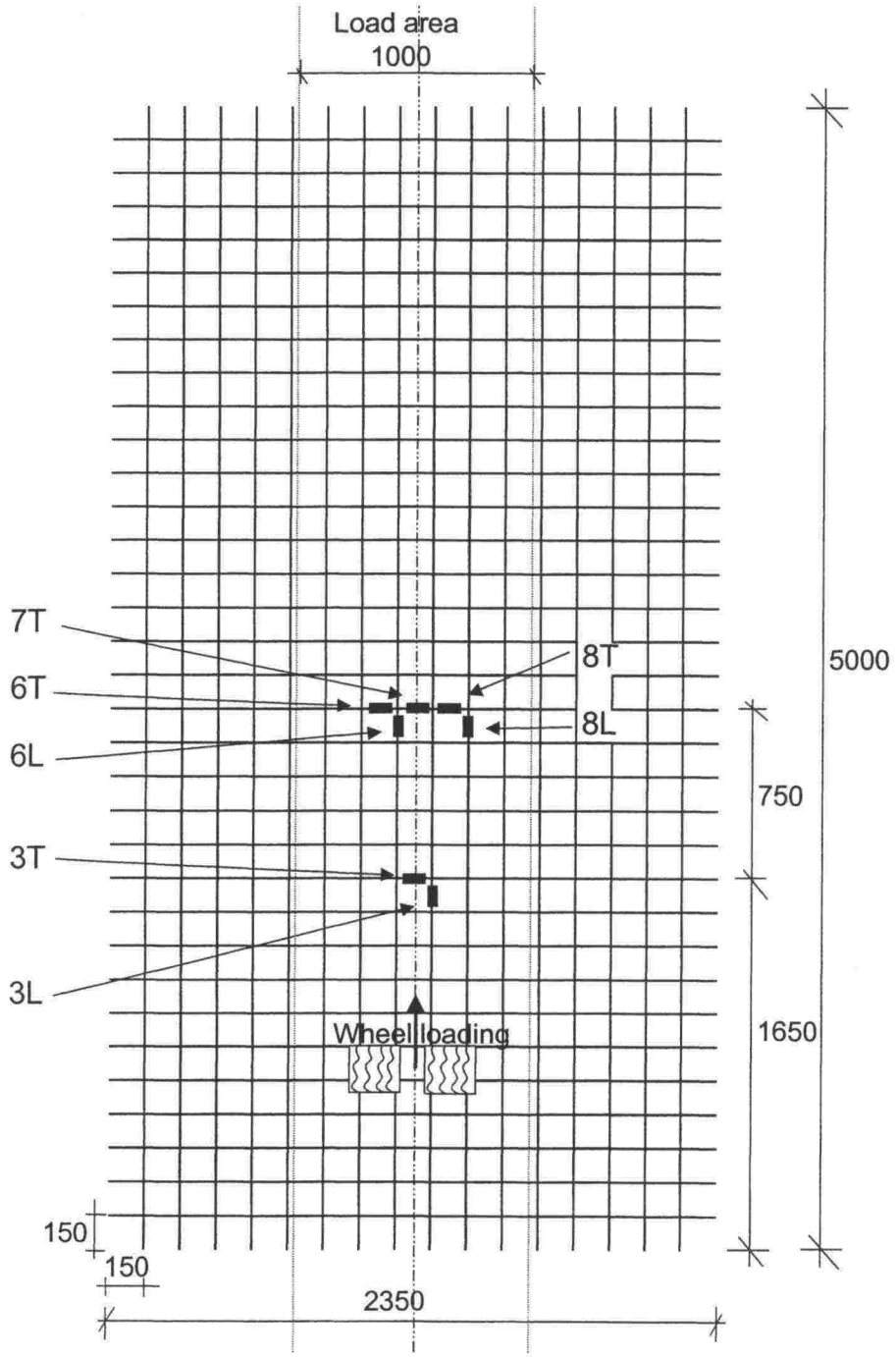

Figure 42. Section C, the centrally positioned steel mesh (see also Fig. 7) and codes for those strain gauges, which were logged during testing.

Table 11. Section C, measured peak strains in steel bars. Applied wheel load was 40kN, with the path along the centreline (see Fig. 42).

code	Initial measurements		Number of passes 6250, rut depth 40 mm		Stress change	Stress change
	Peak tensile strain	Peak tensile stress, σ_0	Peak tensile strain	Peak tensile stress	$\Delta\sigma$	ratio
	μS	MPa	μS	MPa	MPa	%
H3L	163.3	32.7	212.3	42.5	9.8	30
H3T	145.9	29.2	194.4	38.9	9.7	33
H6L	220.4	44.1	212.3	42.5	-1.6	-4
H6T	160.2	32.0	196.4	39.3	7.2	23
H7L	137.2	27.4	180.1	36.0	8.6	31
H8L	115.8	23.2	194.9	39.0	15.8	68
H8T	194.9	39.0	231.2	46.2	7.3	19

In Table 11, the tensile stresses were calculated using Hooke's law ($\sigma = E\,\varepsilon$). The elastic modulus of steel was assumed to be 200GPa. In the table, the measured peak strains were generated at a slightly different moment of time, and the presented values could not considered as the total stress of moment. According to the measurements, the stresses were lower than the yield stress of steel and permanent damage was not generated. It could be seen that, when the pavement had rutted, additional stress was induced in the steel bars (the stress increase per bar was up to 68%). Rutting was also not as fast in Section C as in Sections A and B (see Chapter 4.8).

4.8 Rutting and deformations

4.8.1 Rut development

The development of rutting was measured with a laser-profilometer, made by the Swedish National Road and Transport Research Institute (VTI). Profiles were measured across the loading surfaces at one-metre intervals (Fig. 43).

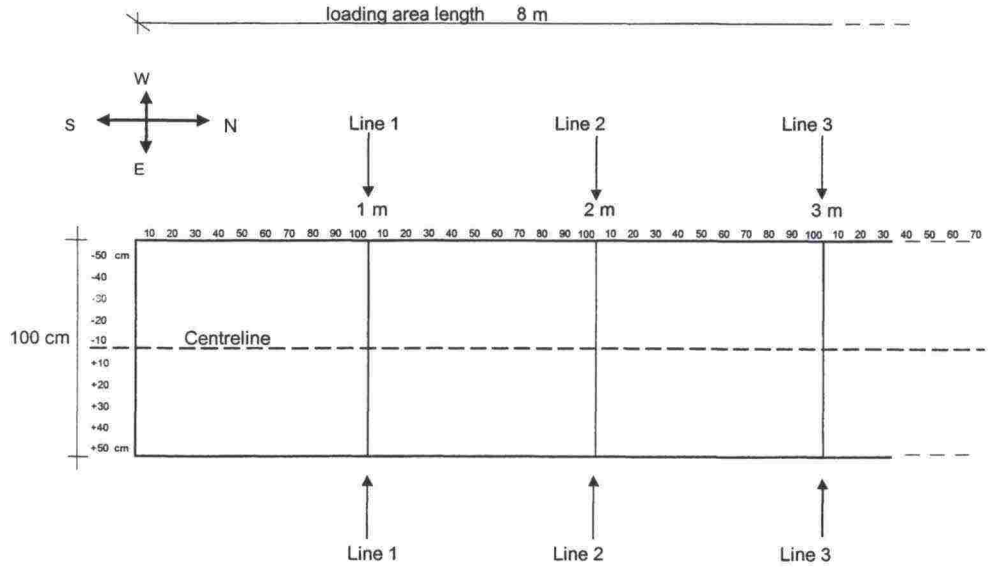

Figure 43. Measurement lines in the tested sections.

An example of rut development in Section B (Line 4m) is illustrated In Fig. 44.

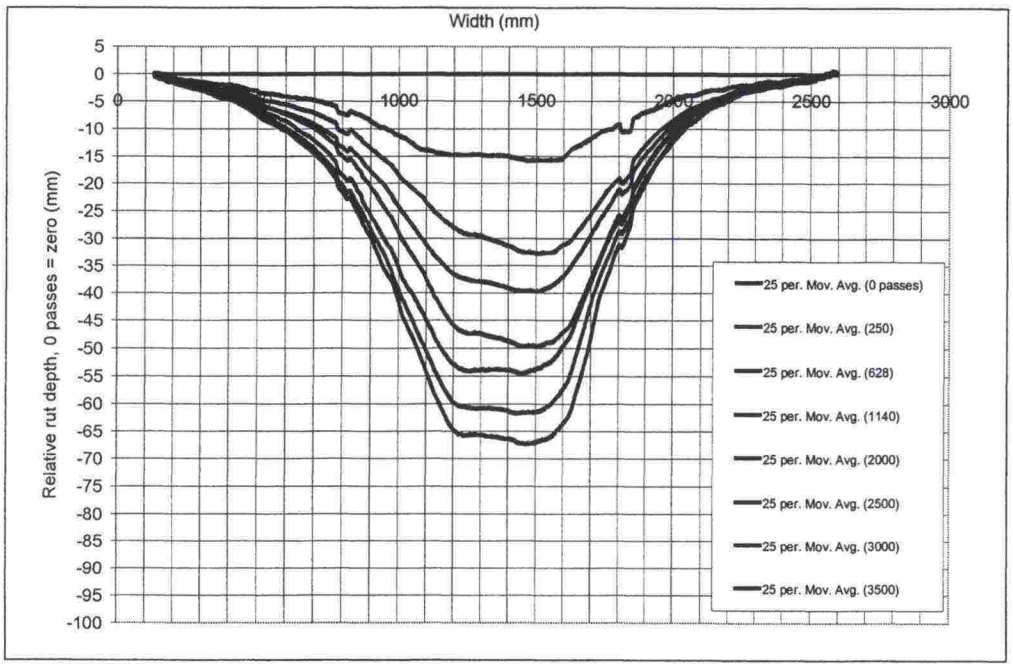

Figure 44. Rutting in Section B; the measurement line was 4th. The developed ruts are relative deviations from the initial surface profile (before pre-loading).

The deepest rut was determined as the largest deviation from the initial surface (before pre-loading, Fig. 45). The measured deepest rut development in Section B is illustrated in Figure 46.

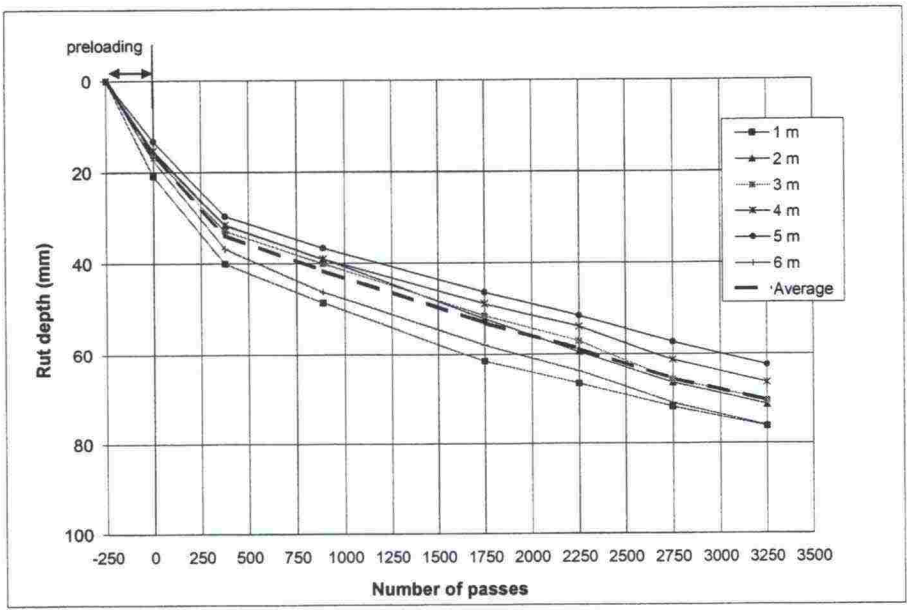

Figure 45. Rut-depth development on different measurement lines in Section B. Rut development during the pre-loading is included in this chart.

4.8.2 Rutting

The rut development in the different sections is illustrated in Fig. 46. Pre-loadings were run with a 20kN wheel load, thus it is irrelevant to count these loads the same as the heavier initial measurement and test loads. The total number of passes was so low that the pre-loadings could distort the total effective overpasses. Hence from then on, the ruts that had developed during the pre-loadings were not included in the total number of passes.

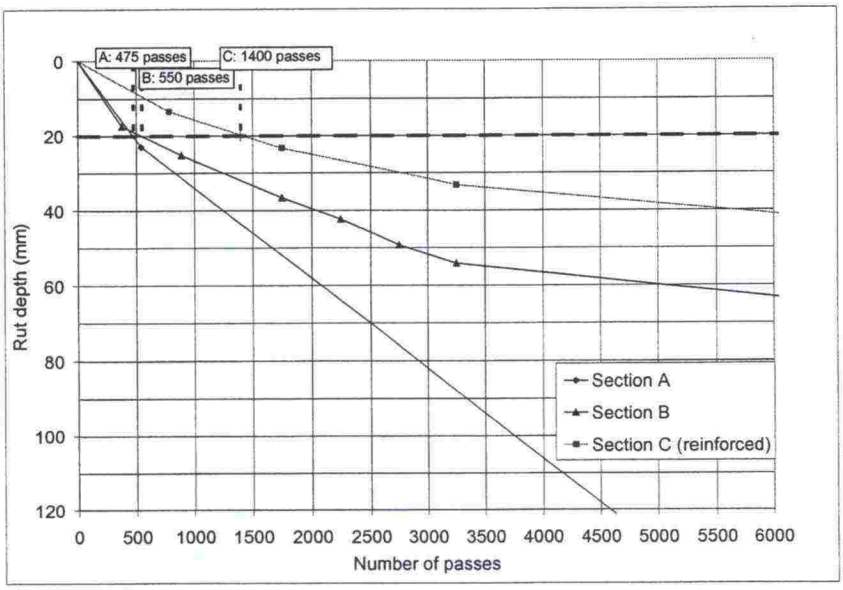

Figure 46. Average rut depth vs. number of overpasses. Damage limit is 20 mm. Pre-loadings are not included.

Rutting on Section C was all the time smaller than on the non-reinforced sections. A 20mm rut depth was reached on Sections A and B during the initial measurements. Section A was tested with a 50kN load, but a 20 mm rut depth was reached before the heavier load could be started. This can be seen as faster deformation after the zero measurements (Fig. 46, about N=500). The initial measurements were quite similar and the results are comparable. However, the test beam side positions did not correspond to the normal test deviation presented in Fig. 12 (Chapter 3.3.1). During the initial measurements, the wheel position was also aligned to positions 0 (centreline) and –15 cm.

The plasticity (or rutting) rate of the tested structures versus the number of passes could be calculated from the profile measurements. The values are presented in Fig. 47. It could be seen that, at the beginning of tests, the plasticity rate was high and the rate decreased during tests. The results from Section A are inadequate.

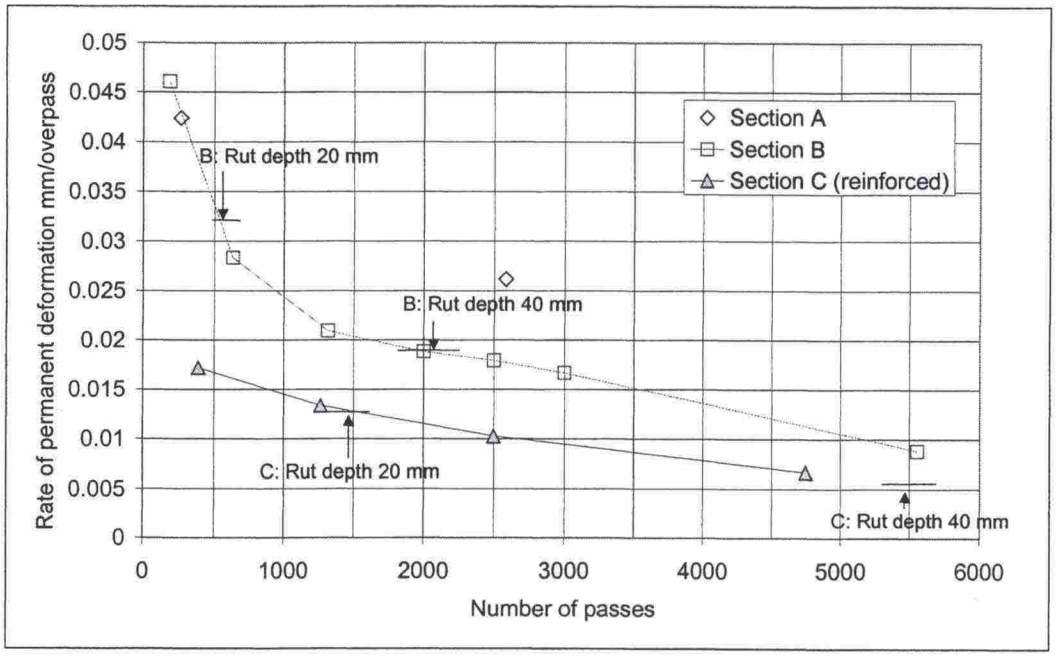

Figure 47. Rate of permanent deformation (mm/overpass) vs. number of passes without pre-loadings.

4.9 Strains in asphalt and crack development

The measured asphalt strains in the bottom of the AC and the observed surface cracks vs. number of overpasses are illustrated in Fig. 48. Heavy wheel loads caused large strains and displacements. The sections rutted so quickly that cracks could not be considered as fatigue cracks. The tensile stress at the bottom of the asphalt concrete exceeded the material strength. This caused a fast development of cracks at the bottom of the bound layer and deterioration of the overall pavement.

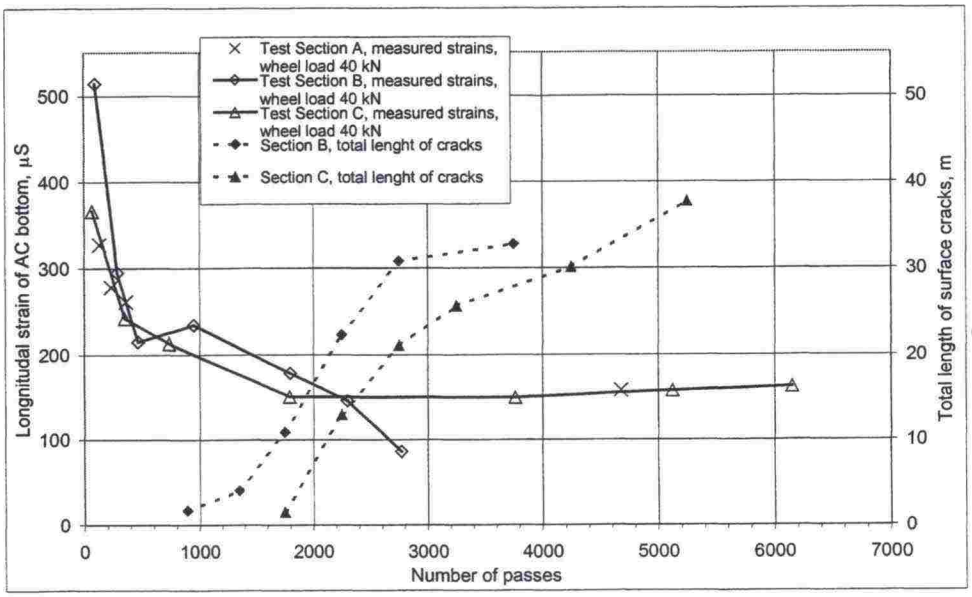

Figure 48. Measured longitudinal strains in bottom of asphalt concrete and total length of surface cracks in tested sections vs. number of passes without pre-loadings in Sections B and C. Crack development was not mapped in Section A.

According to the strain measurements, the tensile strains tended to decrease after the start of loading. The first cracks at the surface of the AC were detected after the bottom tensile strains had dropped. Cracking reduced the stiffness of the AC slab, and thus the stress influence in the base layer was increased.

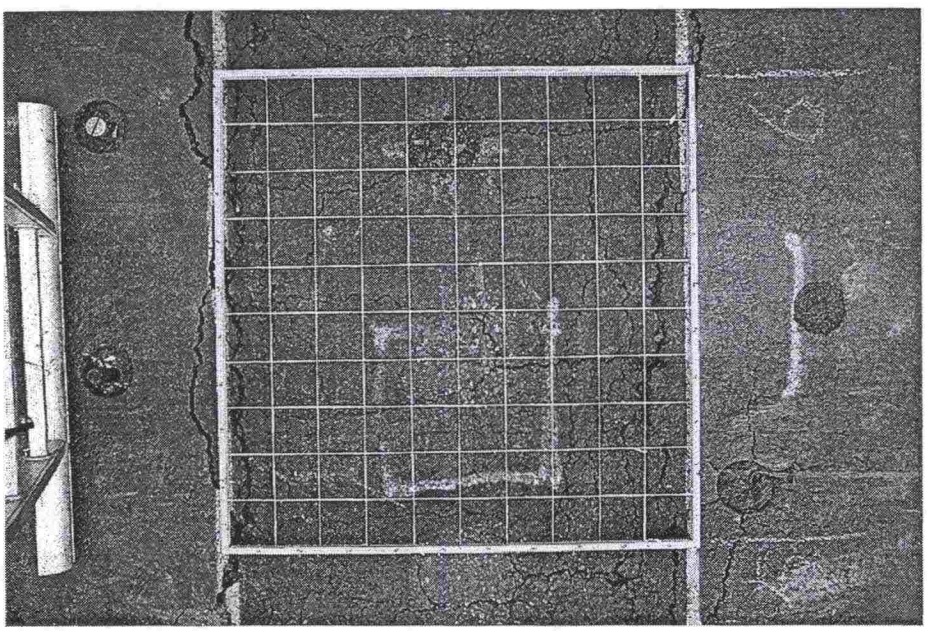

Figure 49. Cracks in Section A after test. Dimensions of mapping mesh are 1x1m.

An example of the measured initial state of asphalt strain in the bottom of the AC is presented in Fig. 50. A clear compression (negative) strain could be seen to precede the large tensile strain.

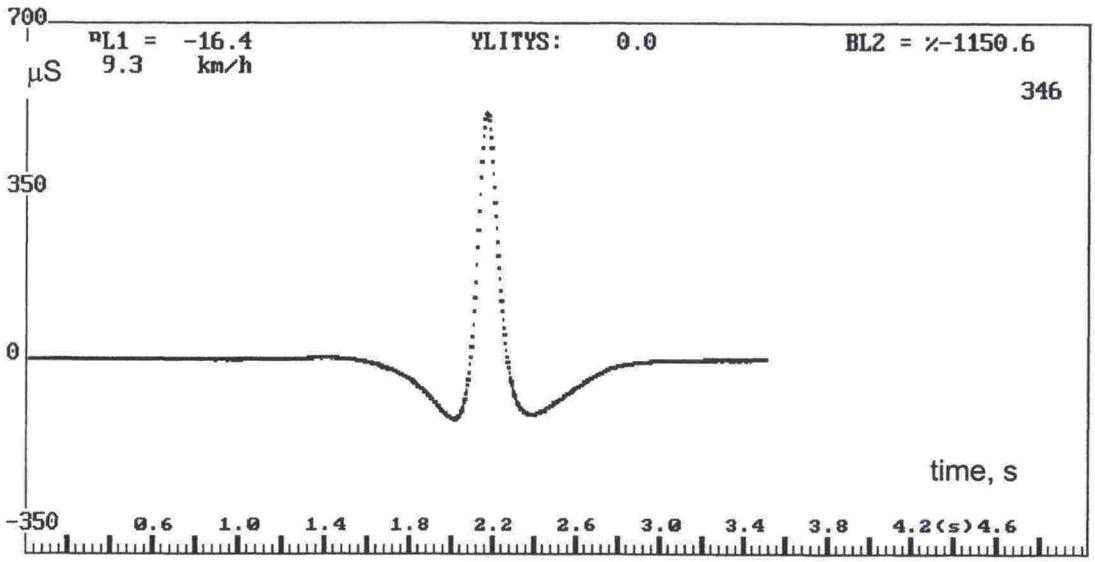

Figure 50. Section B, measured longitudinal strain in the bottom of asphalt during initial measurements, N =96. Wheel load was 40kN.

The asphalt strains, which were measured with the same gauge and with the same loading parameters after wheel loading, are presented in Fig. 51. It can be seen that compression strain had disappeared and tensile strain dramatically decreased after serious rutting and cracking. This indicates that the deformation resistance of the asphalt had decreased.

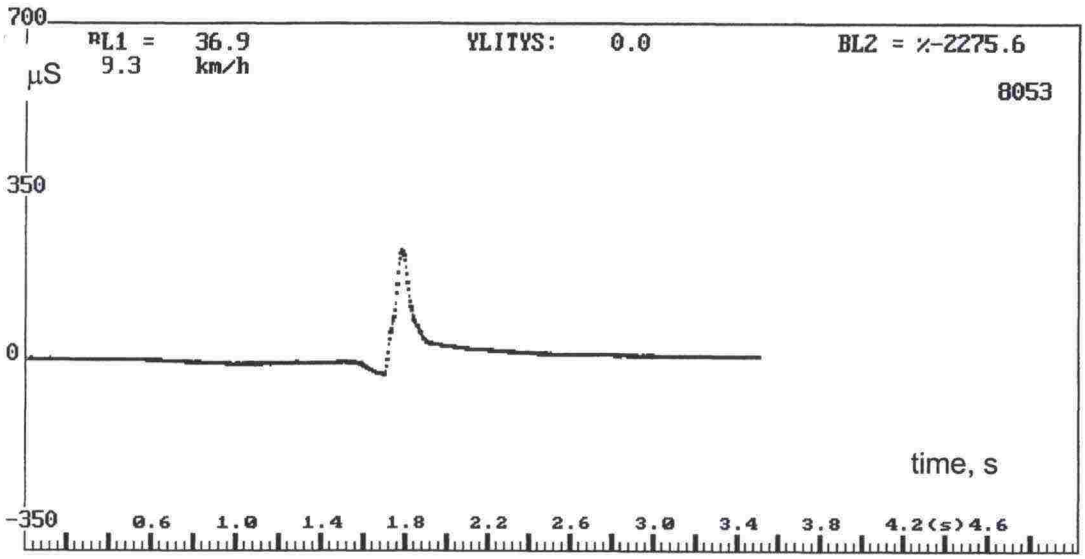

Figure 51. Measured longitudinal strain in the bottom of asphalt, N=7803. Parameters were the same as in Fig. 50.

5 MODELLING AND ANALYSIS

5.1 Modelling pavement stiffness during thaw

The modelling of the test sections was based on in-situ measurement results. The measured FWD deflection bowls were modelled with an 'explicit finite-difference' computer program (FLAC 3.40) /1/. The element grid is presented in Fig. 52.

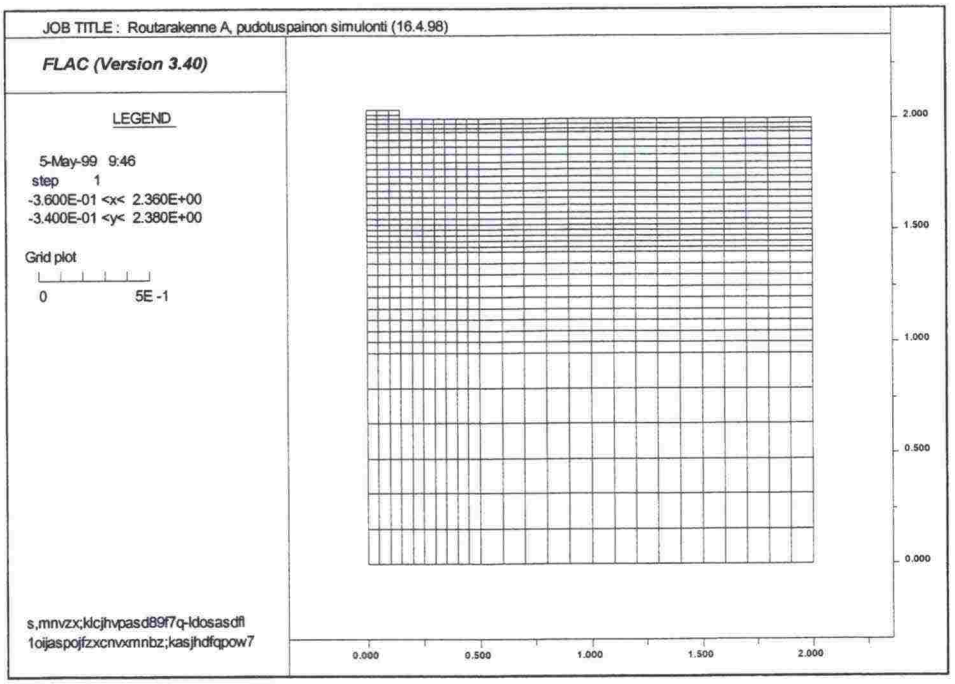

Figure 52. Section A, element grid applied in FWD deflection bowl analysis.

Modelling resulted in a low material modulus of the thawed subgrade (Table 12). A linear elastic model was applied for all the layers. The elastic model was quite simple, but when the aim was to model 'resilient' modulus, the elastic model seemed to give a good equivalence.

Table 12. Estimated material characteristics for different layers in the tested sections.*

Layer	h_A mm	h_B mm	E MPa	ν -
1. Surface	60	60	2000	0.35
2. Base	200	150	50	0.35
3. Subbase	190	195	20	0.35
4. Thaw subgrade	150	448	1.5	0.49
5. Frozen subgrade	450	350	120	0.35
6. Unfrozen subgrade	950	797	30	0.49

*) $h_{A,B}$ thickness of layer (Sections A and B)
E elastic modulus
ν Poisson ratio

The measured and modelled FWD deflection bowls on Sections A and B are illustrated in Figures 53, 54 and 55. In Figures 54 and 55, the modelled bowl is marked with a dashed line and the set of measured deflection bowls are marked with solid lines. The deflection bowls were measured on the test areas at one-metre intervals. The modelled moduli were average estimates for each layer. In the modelling, the applied load was the same as the highest applied FWD load (about 34 kN / 480 kPa).

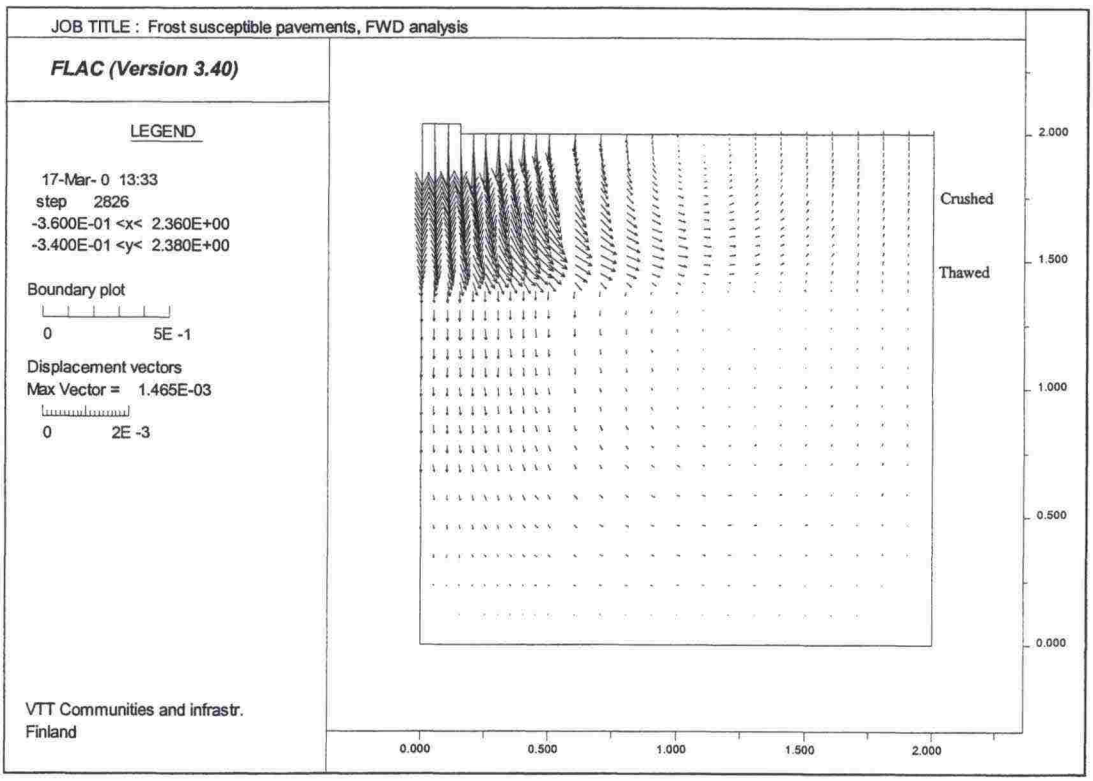

Figure 53. Modelling of FWD deflection bowl. Calculated total displacements of the pavement (Section B), applying the characteristics of Table 12. Surface load was 34kN.

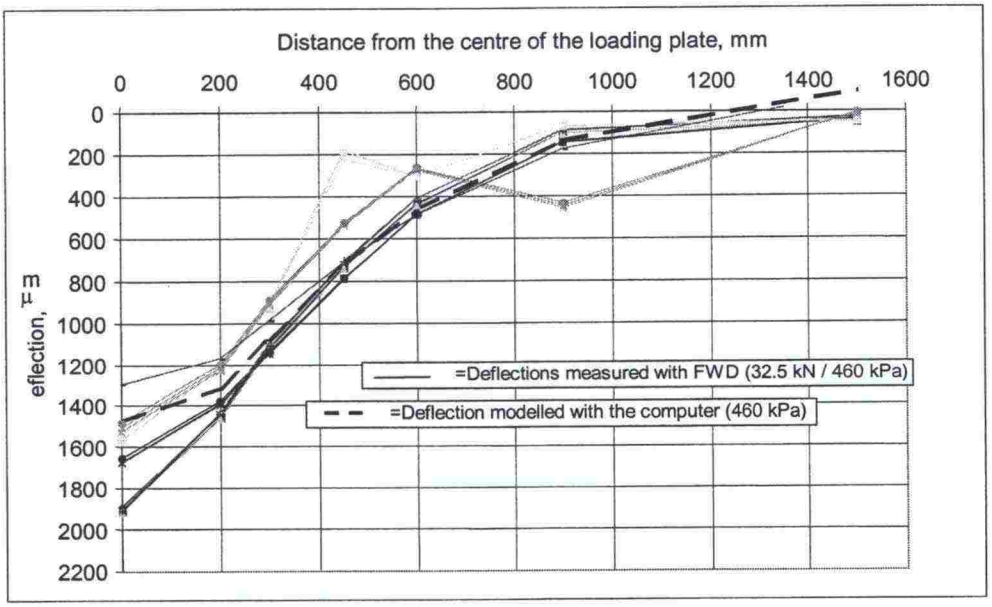

Figure 54. Measured (FWD) deflection bowls on Section A before testing (16.4.1998). The modelled bowl is marked with a dashed line.

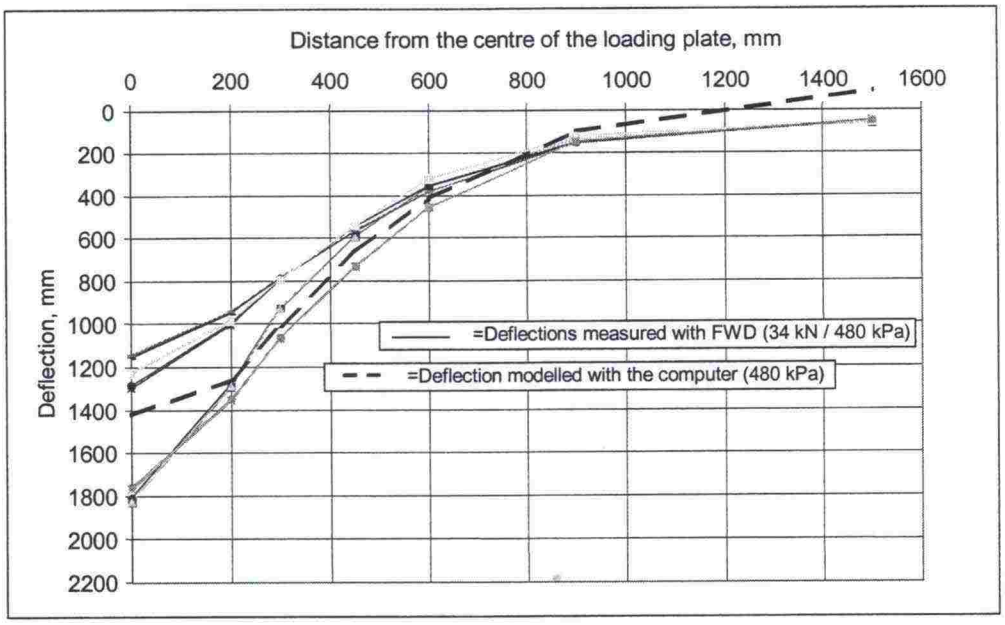

Figure 55. Measured FWD deflection bowls on Section B before testing (7.5.1998). The modelled bowl is marked with a dashed line.

The FWD deflection bowls were measured with three different falling weights. The linear elastic model seemed to correspond quite well at all these stress states. In the preliminary analysis, the traditional MLT (Multi-Layered elastic Theory) computer programs (Bisar and Kenlayer) were tested. The modelling of partially thawed and frozen clay above the unfrozen sub-clay was found to be complicated and the modelling results were unsatisfactory.

5.2 Modelling for pavement and subgrade responses under wheel loading

5.2.1 Modelling earth pressure

Excess earth pressure was also modelled with FLAC /1/. The thawed subgrade was considered to behave according to the undrained elastic model. The frost and thaw penetrations corresponded to the conditions during the measurements. The material parameters were the same as in the FWD analysis (Chapter 5.1). Figure 56 shows the modelled level curves of excess earth pressure with 40kN circle-shaped surface load (r=0.15 m). The measured pressures are also illustrated at their supposed positions.

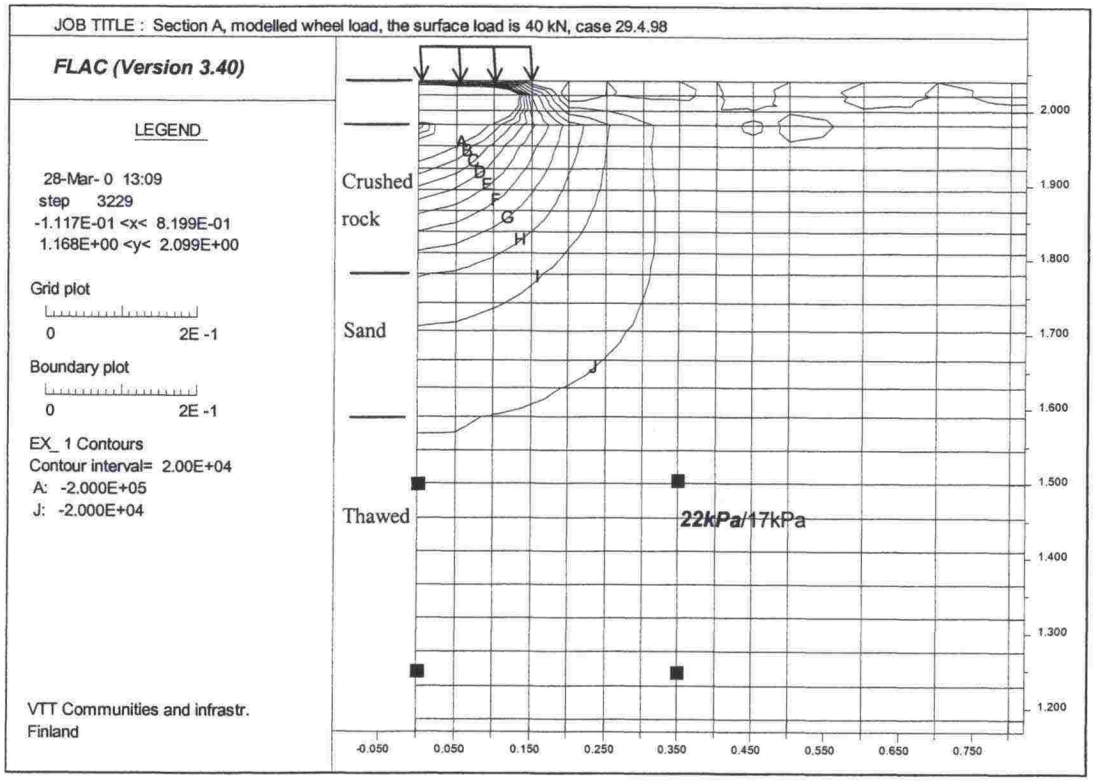

*Figure 56. Section A. Modelling of vertical excess earth pressure. The pressure is modelled with a 40kN surface load. The contour interval is 20kPa (A=200kPa - J=20kPa). The cell positions are illustrated as black rectangles. Measured and modelled pressure increments are beside them (***measured value***/modelled value).*

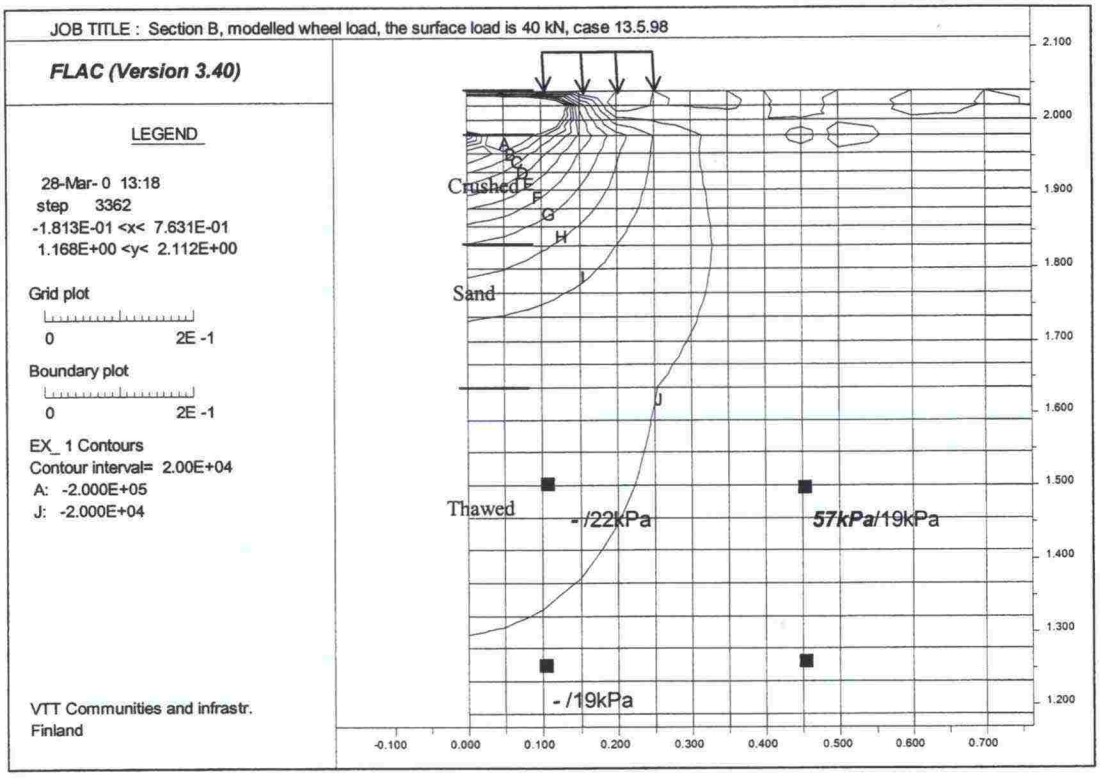

*Figure 57. Section B. Modelling of vertical excess earth pressure. The pressure is modelled with a 40kN surface load. The contour interval is 20kPa (A=200kPa - J=20kPa). The cell positions are illustrated as black rectangles. The measured and modelled pressure increments are beside them (***measured value***/modelled value).*

The measured and analyzed values were quite different. The reason for the difference was probably technical or an inaccuracy in supposed mounting depth.

5.2.2 Modelling transient pore pressure

The excess pore pressure was modelled with Plaxis (ver. 7.1) /2/. The material parameters were the same as in the previous analyses. The thawed clay was considered to be undrained. The level curves of excess pore pressure with 40kN circle-shaped surface load (r=0.15 m) are presented in Fig. 58. The model is for Section B.

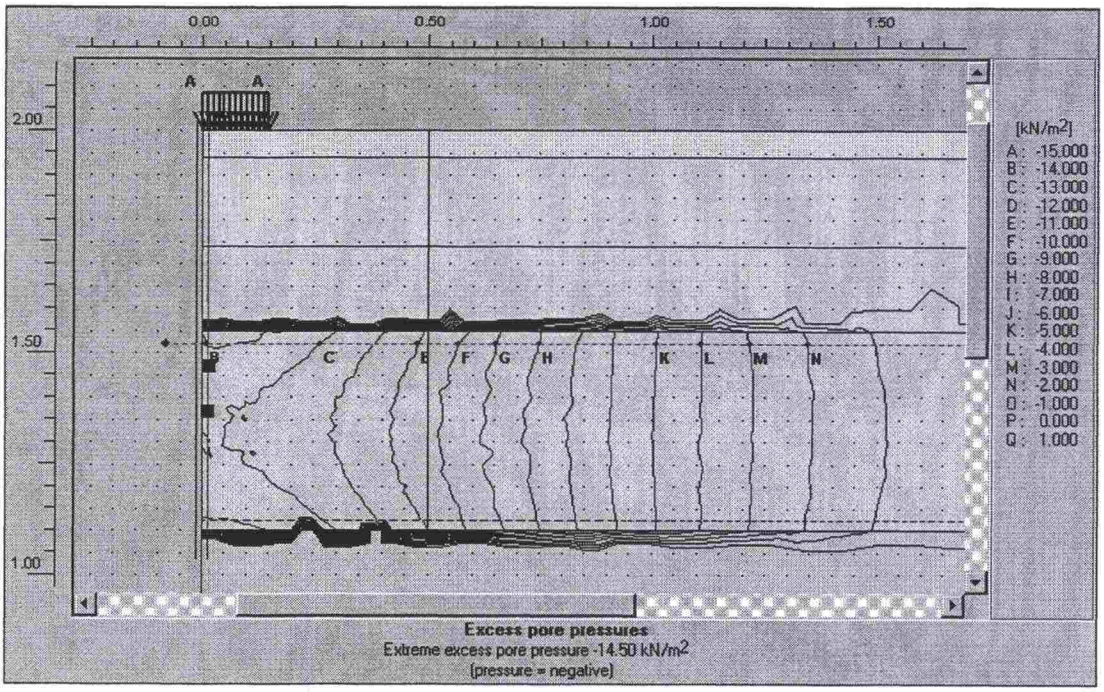

Figure 58. Section A, contour lines for excess pore pressure.

The measured (during initial measurements) and modelled excess pressures in different sections are presented in Table 13.

Table 13. Excess pore pressures with 40kN load.

Section	Code	Depth m	Measured kPa	Analysed kPa
A	FG2	0.60	13	13
	FG1	0.80	5	14
B	GH4	0.65	19	15
	GH3	0.85	17	17
C	HG6	0.63	29	14
	HG5	0.82	(frozen)	15

According to the modelling and measurements, the excess pore pressure was as large as the normal (or octahedronic) stress increment. Under wheel loading, the pore water did not discharge during a transient stress pulse. This confirmed undrained conditions. In Section C, the measured and analyzed values differ from each other.

5.3 Analysis of deformations

5.3.1 Resilient deformations

Resilient deformations under applied load were modelled with FLAC and Plaxis. Both programs seemed to give quite similar results with the same linear elastic layer models. The applied layer characteristics were the same

as in the previous analyses. Frost and thaw penetration corresponded to the conditions during the measurements. The displacement vectors under a 40kN circle-shaped surface load (r=0.15 m) are illustrated in Fig. 59. The example is for Section A. The deformed mesh for section B is illustrated in Fig 60.

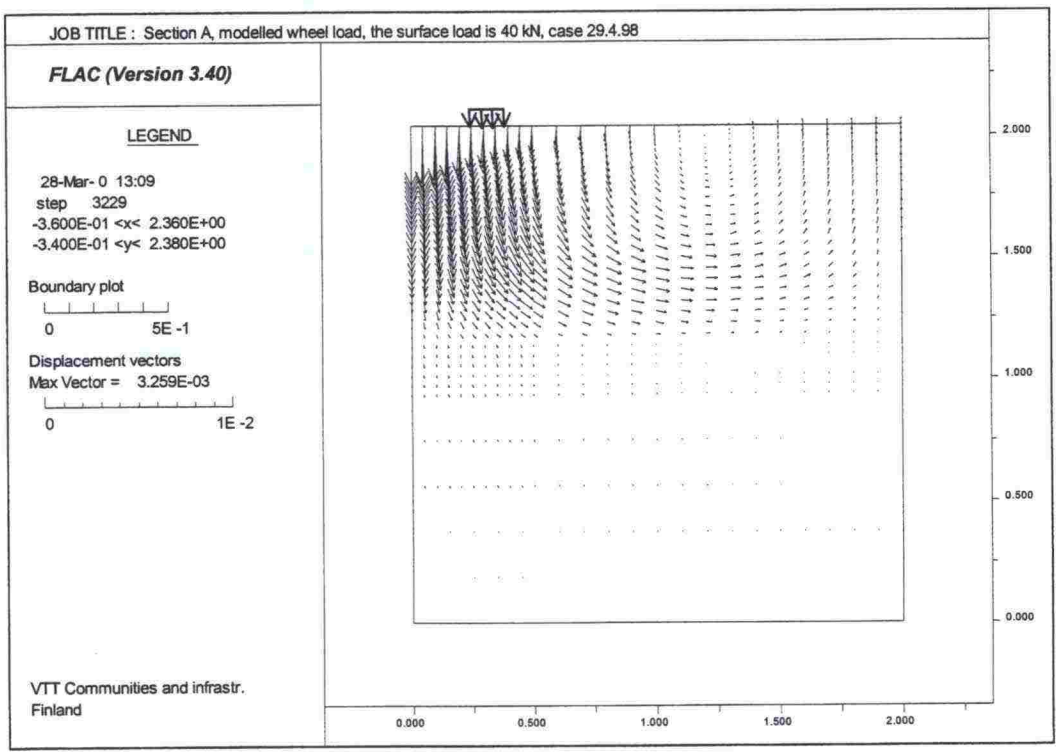

Figure 59. Modelled relative displacements (Flac) with a 40kN surface load in Section A.

The wheel-type was a single one in the modelling, but the actual test wheel was a dual-type. This had to be taken into consideration in determining the equivalent single-wheel load (ESWL). According to Huang (1968), in a two-layered system, the coefficient of equivalence approaches 1, if the subgrade is many times weaker than the pavement /3/. If the aim was to investigate subgrade response, the shape and size of the loaded surface did not have so much of an effect.

In Section C, the steel mesh was modelled by applying a higher material modulus of the crushed rock, corresponding to the same surface deflection as measured on the pavement. In the analysis, the modulus of crushed rock was increased during calculation, until the modelled and measured surface deflection mutually corresponded. Using the elastic model, the equivalent modulus of the crushed rock layer was about 100–300 MPa. This was high compared to the other layers in Section C. The estimated modulus for un-reinforced crushed rock was about 50MPa (see Table 12 in Chapter 5.1). Also, in the elastic model, high tensile stress was generated at the bottom of the crushed rock layer. In Section C, this stress was taken by the steel net, which prevented excess deformations in the unbound material.

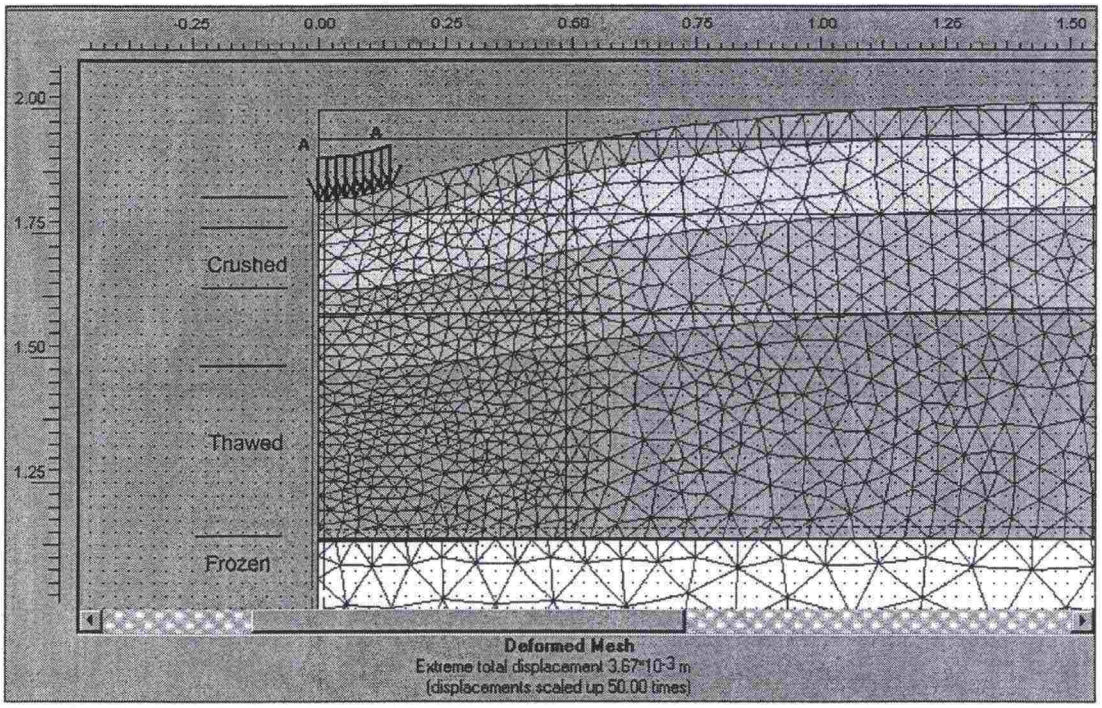

Figure 60. Section B. Modelled deformed mesh (Plaxis) with relative displacements.

The measured and modelled results are presented in Tables 14 and 15.

Table 14. Modelled and measured parameters for different sections.

		HVS test, number of passes at 20/40mm rut		Measured initial deflection of the pavement surface under 40kN wheel load (initial measurements)	Modelled initial deflection of the pavement surface, 40kN
Section	N_{total}	$N_{(20mm)}$	$N_{(40mm)}$	Δ_{tot} (mm)	Δ_{tot} (mm)
A	4702	475	1250	3.36 (1	3.23
B	7851	550	2050	3.96 (2	3.59
C	6288	1400	5550	1.85(1/2.95 (2	1.85/2.90(3

1) deflection gauge
2) Benkelman beam
3) Modelled with two modified moduli of crushed rock 300/100 MPa.

Table 15. Modelled initial pavements. Initial strains and deflections were gained on the surface of the subgrade corresponding to the 40kN wheel load.

Section	Modelled vertical strain	Modelled shear strain	Modelled deflection of subgrade surface	Modelled deflection ratio
	ε_{sub}	γ_{sub}	Δ_{sub} (mm)	$\Delta_{sub}/\Delta_{tot}$
A	0.0131	0.00254	1.74	54 %
B	0.0155	0.00306	2.04	57 %
C(1	0.0110 / 0.0142	0.00160 / 0.00257	1.16 / 1.66	63 % / 57 %

1) Modelled with two modified moduli of crushed rock 300/100 MPa.

5.3.2 Permanent deformation

As a trend-setting method, permanent deformation was analyzed as follows. On tested sections, the deflection of the subgrade surface versus number of HVS overpasses corresponding to the rut depth of 20 mm is illustrated in Fig. 61. It is necessary to remember that the subgrade deflection was not directly measured during the test, because such transducers were not available. The modelling of the responses was covered in Chapter 5.3.1. The problem was to determine the shape of the lifetime curve. The reference curve was taken here from the AASHO test roads, modelled by Ontario Ministry of Transportation and Communications /4/. Additional discussion is presented in Chapter 6.

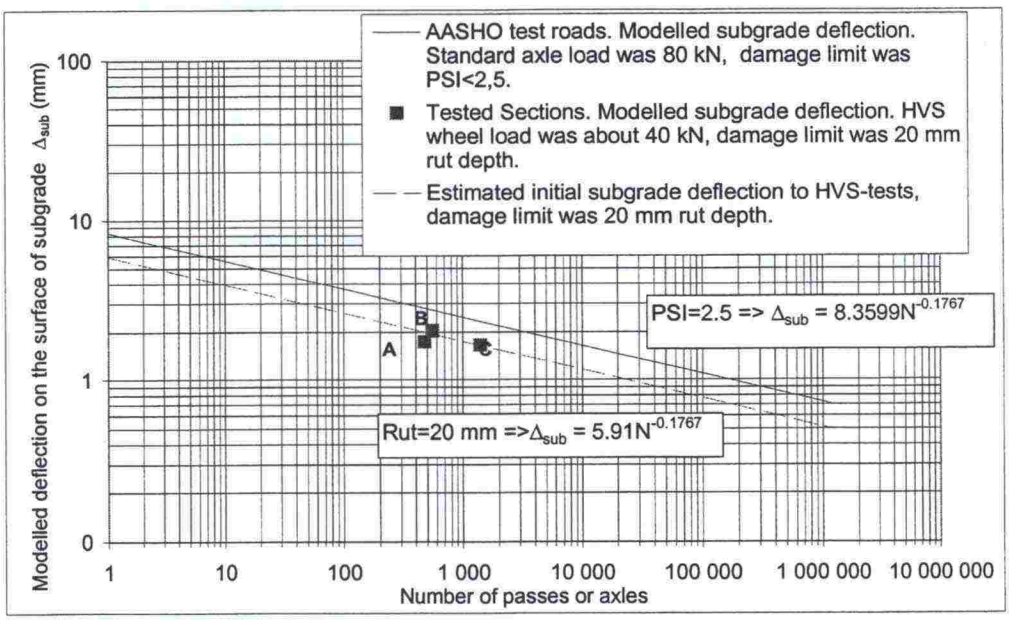

Figure 61. Number of passes vs. modelled initial deflection on the surface of subgrade in HVS-test and in AASHO test roads /4/.

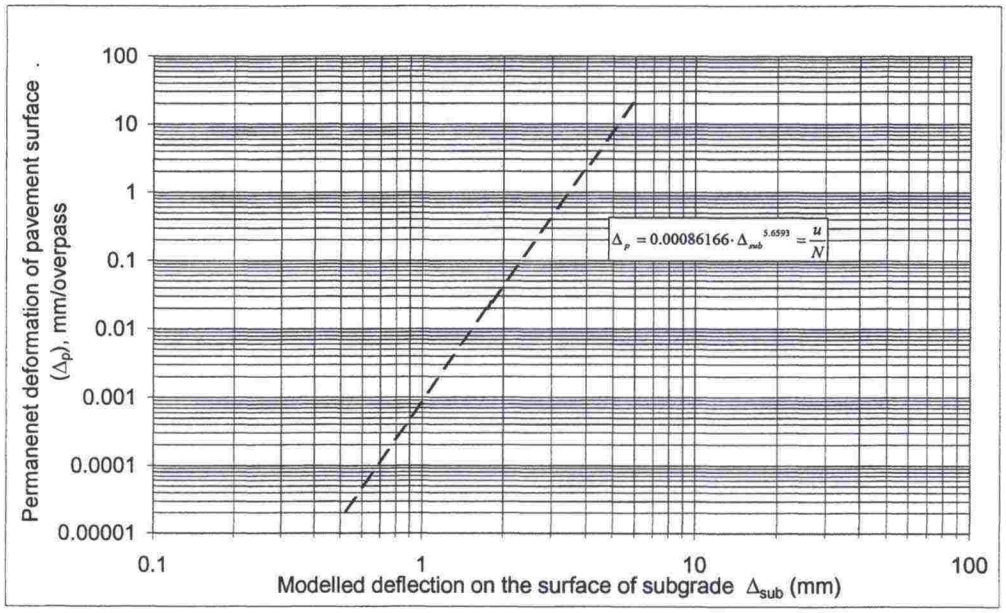

Figure 62. According to the HVS test; the permanent vertical deformation of the overall pavement vs. modelled initial deflection of subgrade surface.

The irreversible, permanent deformation of the overall pavement increases very nonlinearly with the increase of subgrade deflection. Permanent deformation vs. analyzed subgrade deflection is linear, when the relationship is presented in a log-log-scale. The permanent vertical deformation of pavement (increase of rut depth per one HVS overpass) vs. the deflection of subgrade surface, corresponding to the rutting criterion of 20 mm is illustrated in Fig. 62. The data of Figs. 61 and 62 is also presented in Table 16.

Table 16. HVS test, modelled deflection of subgrade surface and the corresponding strain at the number of passes resulting in total rut depth of 20 mm.

Number of overpasses N, resulting rut depth 20mm	Modelled deflection of the subgrade surface, Δ_{sub} (mm)	Modelled vertical strain of the subgrade surface, ε_{sub}
800	1.8	0,015
1 174 500	0,5	0.0042

The relationship between the permanent deformation of the pavement and the deflection of the subgrade is of form (Eq. 1).

$$\log \Delta_p = a \log \Delta_{sub} + b \quad (1)$$

where

Δ_p is the increase of permanent deformation (pavement surface) under applied wheel load

Δ_{sub} is the deflection on the surface of subgrade under applied wheel load

a,b coefficients.

This means that the relationship is exponential, and follows the form of Eq. (2).

$$\Delta_p = e^b \cdot \Delta_{sub}{}^a \quad (2)$$

The interpolated relationship between the rut depth and the deflection of subgrade in Fig. 62, is presented in Eq. (3).

$$\Delta_p = 0.00086166 \cdot \Delta_{sub}{}^{5.6593} = \frac{u}{N} \quad (3)$$

Where

u is total rut depth in mm, and

N is the number of HVS overpasses (with the applied wheel load of about 40kN)

In the analysis of the HVS tests, the initial vertical compressive subgrade surface strain of 0.015 corresponded to the initial subgrade surface deflection of 1.8mm using a wheel load of 40kN. If the ratio of subgrade surface deflection and subgrade strain is assumed to be constant, then the ratio is Eq. (4).

$$\Delta_{sub} = 120 \cdot \varepsilon_{sub} \quad (4)$$

Where

ε_{sub} is the vertical compressive strain on the surface of subgrade, m/m

Substituting Eq. (4) into Eq. (3)

$$\frac{u}{N} = 5.0283 \cdot 10^8 \cdot \varepsilon_{sub}{}^{5.6593} \quad (5)$$

and further

$$u = N \cdot 5.0283 \cdot 10^8 \cdot \varepsilon_{sub}{}^{5.6593} \quad (6)$$

Substituting u=20mm into Eq. (6)

$$N = 3.978 \cdot 10^{-8} \cdot \varepsilon_{sub}{}^{-5.6593} \quad (7)$$

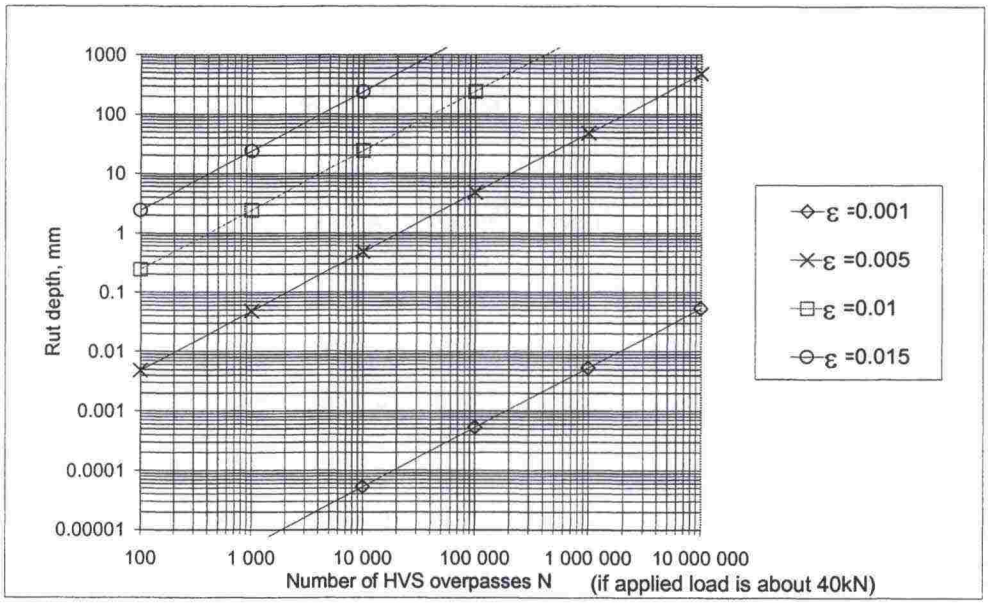

Figure 63. Rut depth vs. number of wheel loadings on assumed vertical compressive strain on the surface of subgrade; 0.001, 0.005, 0.01 and 0.015.

The relationship of Eq. 6 is illustrated in Fig. 63. The rut depth is proportional to the vertical compressive strain on the surface of the subgrade. If the strain is 0.015, then about 800 overpasses cause a 20mm rut depth. A similar rut depth is caused by $3*10^6$ overpasses, if the strain is 0.005, and by $5*10^9$ overpasses, if the subgrade strain is 0.001. The relationship tells us also that if the structure behaves in an elastic manner, and if the pavement structure is the same, then an increase of wheel load is related to the increase of subgrade deformation, and the number of HVS overpasses causing a 20mm rut is decreased to the 5.7^{th} power of wheel load ratio.

The rutting model described above is analogous with the fatigue curves presented in literature for subgrades /5/. In this model, the damage criterion is the rut depth instead of the fatigue damage of the pavement surface

6 DISCUSSION

6.1 The rutting model

In computer modelling, the problem was that an ideal elastic model allows tensile stress at the bottom of unbound layers. Therefore, the moduli between two unbound pavement layers must be chosen correctly to avoid unrealistic tension. The moduli, illustrated in Table 12 (Chapter 5.1), can be considered as the 'functional' or 'effective' modulus of layers. If the thawed clay had been stiffer, the upper layers would have 'functioned' with higher moduli, and the total as well as plastic strains would have been smaller. In addition, the modulus of the pavement layers depends on the applied stress state, and some materials are also visco-elastic. Thawed clay was found to be undrained under a transient load pulse. The FWD deflection bowls were measured with three different falling weights. Linear elastic FEM modelling seemed to correspond quite well to all of these stress states.

The determined moduli are also dependent on the measuring method. The FWD test gives a dynamic response of the pavement, which simulates the real wheel load.

The reference points for the rutting model, which was taken from the AASHO test roads, was presented in Chapter 5.3.2. In the AASHO test roads, PSI=2.5 was used as the lifetime indicator. PSI cannot be compared to the rut depth, but the shape of the lifetime curve was considered to be similar.

It could be seen in Chapter 5.3.2 (Fig. 61), that one 40kN HVS overpass seems to have a heavier load action than one 80kN axle in the AASHO tests. If a rut depth of 20mm occurred in a real road, evidently the PSI would be lower than 2.5 and the curve presented in Figure 61 would be above the AASHO reference curve. The speed of the HVS wheel was 12km/h, which is much lower than normal traffic speed. On the soft subgrade, the impact time was even longer.

The rutting model described in Chapter 5.3.2 presents the unit vertical permanent deformation in a thawing, frost-susceptible subgrade, caused by permanent shear deformation. Shear deformation, on the other hand, is dependent on the creep properties of the subgrade soil and also on the bending stiffness of the pavement structure. The influence of loading is very small, if the deflection is small. The stiffness of the pavement also does not change at a small deflection.

The rutting model may be applied for estimation of pavement rutting provided that subgrade deformations are estimated (or modelled) during the design.

The rutting is exponential with the power of 6. It is based on the fundamental relationship between the total and permanent deformation of the subgrade in cyclic loading with the HVS. In the model, if the stiffness of

the pavement and subgrade is assumed to be constant, the wheel load and total deformation are linearly related. The rutting equation (6) indicates that the rutting is changed to the 6^{th} power related to the change of loading. In addition, the factor between the HVS and normal traffic load should be related. Additional testing should be conducted to further validation.

6.2 Further analysis

The construction and testing of the test pavement was, as such, a rather multi-layered complex. In this report, only first-hand results have been analyzed and discussed. The next, more detailed layers of the 'onion' might be, for instance the following:

- influence of soft underlay on the compaction and stiffness of pavement layers
- analysis of reinforced pavement considering the anchoring behaviour and interaction of the steel mesh in comparison to un-reinforced ones
- analysis of frost heaving
- analysis of thawing and thaw consolidation
- analysis of pore pressures and effective stresses during thaw
- modelling the pavement modulus variation before and during freezing, and during and after thawing
- many other themes.

The detailed analysis and modelling of the tests will help to understand frost action on pavements on frost-susceptible subgrades. The main results, of course, motivated the testing. The full benefit can be gained by proper modelling. The HVS equipment is more a verification facility, and not so much a material testing device. Individual tests are expensive and a more complete analysis of the results should be preferred.

7 CONCLUSIONS

7.1 Testing and results

1. Construction of frost-susceptible subgrade and a good thin pavement on a soft underlay was a challenging task. This could be seen in the layer roughness determined from the trial pits. In addition, there was some uncertainty in the position of the instruments installed during construction. Despite the difficulties, though, the test results could be interpreted as fair.

2. The measured surface moduli were dramatically lower during thaw in comparison with the freezing season. The surface moduli dropped when frozen soil started to thaw, and they were at the lowest when the frozen clay was totally thawed and before the post-consolidation.

3. According to the FWD measurements, the initial surface modulus was not significantly higher in the reinforced Section C compared to the un-reinforced Sections A and B. However, the difference in measured deflections was 40–45 % between Sections C and A with the moving wheel test. The test parameters and thaw penetrations were similar. Also, the rutting resistance was 2.5-fold (with a rut limit of 20mm) compared to the other sections. The steel mesh reinforcement seemed to resist deformation better under moving load.

4. The effect of the steel reinforcement in Section C improved all the time with the increasing rut depth. The measured strains indicated the increasing stress in the steel bars due to rutting. This can be seen as less rutting in Section C.

5. The applied wheel loads (40–50kN) were high considering the tested frost-susceptible pavements with low surface moduli. In addition, the test wheel speed (12km/h) was low compared to normal traffic speeds. Thus, the load impact lasted longer. Further, the loading effect in the subgrade lasted longer. This may have contributed to the fast development of rutting and cracks in the test pavements.

6. Large strains and displacements under the heavy wheel loads caused high tensile stress at the bottom of the asphalt concrete. The material strength of asphalt was exceeded. This caused a rapid development of cracks at the bottom of the bound layer. The measured tensile strains started to decrease after the beginning of the test loading. The first cracks in the surface of the asphalt concrete were detected after the bottom tensile strains had been lowered. The cracking lowered the pavement response and increased the stresses and strains in the subgrade. The deformations in the base layer were increased as well.

7.2 Modelling and analysis

7. Based on the modelling, because the overlay was relatively thin, the critical location of deformations was probably the surface of the soft subgrade. The material modulus of the thawed clay was low, and deflections under wheel loads became high. Presumably most of the deformations developed in the thawed clay. This caused the fast deterioration of the overall pavement.

8. The moving test wheel caused a fast stress pulse in the soil. Under undrained conditions, this developed a transient pore pressure increment in saturated clay. Excess pore pressure reduced the shearing resistance and stiffness of clay. It was also observed that cyclic loading increased the level of total pore pressure. The static pore pressure was at a lower level before the non-stop cycle than after the loading period. The interval during cyclic loading (amplitude) was about 7 sec.

9. The soft base layer with large displacements limited the material modulus of the unbound overlay. Theoretically, the unbound overlay can have only a certain reduced effective material modulus on a soft base.

10. Only FEM based computer programs were used, and the results may differ from those that can be modelled with MLT-based programs.

11. The modelling presented in this report is validated only on tested frost-susceptible sections. Rutting can be dependent on the subgrade material and additional testing should be conducted for further validation.

8 LITERATURE AND REFERENCES

This document was selectively translated and edited from documents:

Saarelainen S., Onninen H., Kangas H., 1998, *HVS testing of pavements on thawing frost-susceptible subgrade* (In Finnish) Technical Research Centre of Finland, project report RA10.

Kangas H., *Testing of a pavement on thawing, frost-susceptible subgrade with the Heavy Vehicle Simulator (*In Finnish with English summary*),* Helsinki University of Technology, Department of Civil and Environmental Engineering, Diploma thesis. 100 p. Espoo, Finland 1999

Additional reference literature

1. Itasca consulting group Inc., 1998, FLAC - Fast Lagrangian Analysis of Continua version 3.40 User's manuals, Minneapolis, Minnesota, USA.
2. Brinkgreve R.B.J., Vermeer P.A., 1998, Plaxis – Finite Element Code for Soil and Rock Analyses version 7 (manual), Plaxis BV, AB Rhoon, Netherlands
3. Huang Y.H., 1968, *Chart for determiningg equivalent single wheel loads*, Journal of the Highway Division, ASCE, Vol 94, No HW2, pp. 115-128.
4. Ontario Ministry of Transportation and Communications, 1975, *Elastic layer analysis related to performance in flexible pavement design*, RR191, Toronto, Canada.
5. Korsu P., Belt J., Ehrola E., 1995, *E-moduli and deformation lines of subgrades* (in Finnish), Finnra, internal publications 59/1995 44p.+8app.

ISSN 0788-3722
ISBN 951-726-661-8
TIEL 3200619E